Results from PNNL SCC Testing: FY20

Spent Fuel and Waste Disposition

Prepared for
US Department of Energy
Spent Fuel and Waste Disposition

M.B. Toloczko
R.A. Bouffioux, F.C. Colon

Pacific Northwest National Laboratory

September 11, 2020
M2SF-20PN010207048
PNNL-30368

SUMMARY

In FY19, a multi-year test plan was created to provide quantitative chloride-induced stress corrosion crack (CISCC) growth rate data on 304 and 316 stainless steel (SS). The central piece of this plan is the use of state-of-the-art in-situ measurement of crack length and an actively managed testing approach to effectively measure CISCC. The program is geared towards providing a strong foundation of baseline testing under well controlled environments to aid in understanding CISCC response. Testing has begun in immersed conditions using compact tension (CT) crack growth specimens. Immersed conditions provide better control over crack tip water chemistry while the use of compact tension specimens, that are the standard for in-situ measurement of crack growth, provides a familiar basis for testing.

After quantifying the SCC response of CT specimens in immersed conditions, a 4-point bend (4PB) geometry with short cracks growing from a flat surface will be adopted because of its better ability to control salt loading on the specimen surface compared to a notched CT specimen. A portion of the CT specimen CISCC growth rate testing matrix in immersed conditions will be duplicated with the 4PB to demonstrate reproducibility with the compact tension crack growth testing data set. Testing will then transition to humid air deliquescent conditions where many of the same environmental and material effects that were evaluated in immersed conditions will be measured again. This stepped approach will provide a strong basis for understanding CISCC response in humid air deliquescent conditions.

Two 6-specimen CISCC test systems were constructed in FY19 and two more were completed in FY20. While PNNL has extensive experience with designing, constructing, and optimizing test systems for evaluating SCC in light water reactor cooling water conditions, CISCC testing was a new topic area, and as a result, much of the chemistry control system and environmentally exposed materials needed to be redesigned for corrosive, concentrated brine solutions. At the same time the two FY20 test systems were being constructed, extended shakedown testing and optimization of the FY19 test systems was performed with the resulting optimizations applied to all four test systems. Optimization efforts targeted improving crack length measurement resolution, achieving uniform water chemistry and temperature in the environmental chamber, and dissolving air into brine water solutions during testing without depositing salt and blocking air flow.

Tests on six specimens were started in FY20 with four of those tests continuing into the next fiscal year. These tests are all being conducted in 40°C, air saturated water that is nearly saturated with sodium chloride. The initial effort has focused on evaluating the effect of stress intensity, and for the two stress intensities evaluated (20 and 25 MPa$\sqrt{m}$) CISCC growth readily takes place at rates ranging from $1x10^{-8}$ to $2x10^{-7}$ mm/s (0.6-5 mm/yr) for 304L SS and sensitized 304 SS. Testing on these specimens will continue at progressively lower stress intensities until CISCC growth rates drop below ~$2x10^{-9}$ mm/s.

The test plan calls for evaluating multiple heats of material, and to this end, large quantities of three different 300-series stainless steels were obtained in FY20, specifically, two heats of 304L and one heat of 316L. These are referred to as task heats of material. One of the key take-aways from service experience in nuclear power plants is that SCC of the reactor pressure boundary that is exposed to reactor high temperature cooling water typically occurs first in regions where the component microstructure has become compromised in some way. This can be due to poor starting microstructure, or more commonly, it occurs in weld heat affected zones and regions with mechanical damage, in particular grinding damage, impact damage, or in components that were plastically deformed during reactor construction. Based on this understanding, the choice was made for CISCC testing to be conducted on materials that are 10% plastically strained. A route for obtaining 10% tensile straining was determined this year, and the first CT specimens of each of the three materials in the 10% tensile strained condition will be available for testing starting around September 1.

Tests on as-received and on 10% tensile strained material from each of the three heats will start before the end of the fiscal year, again continuing with the focus on determining the stress intensity dependence because initial cracks in structures will be at relatively low stress intensities.

This page is intentionally left blank.

ACKNOWLEDGEMENTS

The authors would like to express their sincere thanks to the project's U.S. Department of Energy's sponsor, Ned Larson, for supporting and funding this work. PNNL would also like to acknowledge Charles Bryan and Rebecca Schaller of Sandia National Laboratories along with Darrell Dunn of the US Nuclear Regulatory Commission for discussions on testing ideas.

This page is intentionally left blank.

CONTENTS

LIST OF FIGURES

LIST OF TABLES

This page is intentionally left blank.

ACRONYMS

4PB	4-point bend
AFCGR	air fatigue crack growth rate
CCR	continually cast and rolled
CGR	crack growth rate
CISCC	chloride-induced stress corrosion crack(ing)
CISCCGR	chloride-induced stress corrosion crack growth rate
CMTR	certified material test report
CT	compact tension
CW	cold work
DCPD	direct current potential drop
DCSS	dry cask storage system
FEM	finite element model(ing)
GB	grain boundary
HAZ	heat effected zone
IGSCC	intergranular stress corrosion cracking
K	stress intensity
LWR	light water reactor
NRC	Nuclear Regulatory Commission
PNNL	Pacific Northwest National Laboratory
PWR	pressurized water reactor
PWSCC	pressurized water stress corrosion cracking
SCC	stress corrosion crack(ing)
SCCGR	stress corrosion crack growth rate
SNL	Sandia National Laboratories
SS	stainless steel
TGSCC	transgranular stress corrosion cracking
YS	yield stress

This page is intentionally left blank.

RESULTS FROM PNNL SCC TESTING: FY20

1. INTRODUCTION

Pacific Northwest National Laboratory (PNNL) is leveraging its 15 years of experience performing quantitative stress corrosion cracking (SCC) tests in simulated light water reactor (LWR) cooling environments **[1-3]** to develop a state-of-the-art SCC testing approach for evaluating chloride induced stress corrosion cracking (CISCC) in humid air deliquescent conditions in support of dry cask storage systems (DCSS). In FY19, a multi-year test plan was created to provide quantitative chloride-induced stress corrosion crack (CISCC) growth rate data on 304 and 316 stainless steel (SS) **[4]**. The central piece of this plan is the use of state-of-the-art in-situ measurement of crack length and an actively managed testing approach to effectively measure CISCC under constant stress intensity or constant load. This methodology for measuring cracking is the world standard for evaluating SCC growth rates of nuclear reactor pressure boundary components exposed to high temperature water **[5-7]**. This approach has only been used with limited success for concentrated CISCC growth measurements **[8, 9]**, while there is no evidence of active test management having been previously used with any degree of success for CISCC testing in concentrated solutions or in deliquescent humid air conditions.

The PNNL task is geared towards providing a strong foundation of baseline testing under well controlled environments to aid in understanding CISCC response. Testing begins in immersed conditions using compact tension (CT) crack growth specimens. Immersed conditions provide better control over crack tip water chemistry while the use of compact tension specimens that are the standard for in-situ measurement of crack growth, provides a familiar basis for testing. After familiarity and data are obtained with CT specimens in immersed conditions, a 4-point bend (4PB) geometry with short cracks growing from a flat surface will be adopted because of its better ability to control salt loading on the specimen surface compared to a standard, notched CT specimen. A portion of the CT specimen CISCC growth rate testing matrix in immersed conditions will be duplicated with the 4PB geometry to provide an explicit link to the compact tension crack growth testing data set. After that link has been obtained, testing will then transition to humid air deliquescent conditions where many of the same environmental and material effects that were evaluated in immersed conditions will be measured again. This stepped approach will provide a strong basis for understanding and believing the observed CISCC response in humid air deliquescent conditions.

The goals for FY20 have been to construct two more test systems, perform test system optimizations for CISCC testing in immersed conditions, obtain and prepare materials for CISCC testing, and perform whatever CISCC testing is possible. Despite challenges with being able to perform hands-on lab work due to COVID-19, these goals have largely been accomplished.

Two 6-specimen CISCC test systems were constructed in FY19, and two more were completed in FY20. While PNNL has extensive experience with designing, constructing, and optimizing test systems for evaluating SCC in light water reactor cooling water conditions, CISCC testing was a new topic area, and as a result, much of the chemistry control system and environmentally exposed materials needed to be redesigned for corrosive, concentrated brine solutions. At the same time the two FY20 test systems were being constructed, extended shakedown testing and optimization of the FY19 test systems was performed with the resulting optimizations applied to all four test systems. Optimization efforts targeted improving crack length measurement resolution, achieving uniform water chemistry and temperature in the environmental chamber, and on effectively dissolving air into brine water solutions during testing.

The test plan calls for evaluating multiple heats of material, and to this end, large quantities of three different 300-series stainless steels were obtained in FY20, specifically, two heats of 304L and one heat of 316L. These are referred to as task heats. One of the key take-aways from service experience in nuclear power plants is that SCC of the reactor pressure boundary that is exposed to reactor high temperature cooling water typically occurs first in regions where the component microstructure has

become compromised in some way. This can be due to poor starting microstructure, or more commonly, it occurs in heat affected zones and regions with mechanical damage, in particular grinding damage, impact damage, or in components that were plastically deformed during reactor construction. Based on this understanding, the choice was made for CISCC testing to be conducted on materials that are 10% plastically strained. A route for obtaining 10% tensile straining was determined this year, and the first CT specimens of each of the three materials in the 10% tensile strained condition will be available for testing starting around September 1.

Tests on six specimens made from non-task heats of 304/304L SS in an as-received (non-strained) condition were started in FY20 with four of those tests continuing into FY21. These tests are all being conducted in water saturated with sodium chloride and air at 40°C. The initial effort has been on evaluating the effect of stress intensity, and for the two stress intensity ranges that have been evaluated to-date, (~20 and ~25 MPa$\sqrt{m}$) CISCC growth readily takes place at rates ranging from $2x10^{-8}$ to $1.7x10^{-7}$ mm/s (0.6-5 mm/yr) for 304L SS and sensitized 304 SS. Testing on these specimens will continue at progressively lower stress intensities until CISCC growth rates drop below ~$2x10^{-9}$ mm/s. Tests on as-received and on 10% tensile strained material from each of the task three heats will start before the end of the fiscal year, again continuing with the focus on determining the stress intensity dependence because initial cracks in structures will be at relatively low stress intensities.

2. REVIEW OF SCC AND SCC TESTING CONCEPTS

SCC is a multi-step process in the regard that it includes both crack initiation and growth (Figure 1). The initiation step is typically considered to be comprised of two or more sub-steps that depend on the controlling mechanism. For LWR SCC, this could include elemental redistribution on grain boundaries (GBs), the formation of a leading oxidation front on GBs, and eventually the formation of short cracks. For CISCC, the steps to initiation for a stainless steel may include development of a local corrosion environment, pit formation and growth, and then crack nucleation from a pit. Cracking may also nucleate from surface irregularities that produce stress risers and localized crevice chemistry, all of which are often associated with non-optimal material condition. The definition of an initiated crack is dependent on perspective. In terms of physical presence, initiation can be the point at which an observable crack forms, however, the ability to resolve a crack is dependent on the examination technique. Cracks with an opening as narrow as 30 nm are resolvable by scanning electron microscopy under some conditions while resolution by optical methods could require an opening >500 nm. Rather than define initiation by some physical attribute of the crack (e.g., a minimum crack opening, length, or depth), PNNL denotes the point of initiation as the time at which nucleated cracks begin to grow more rapidly into a specimen. After a crack has formed to a certain depth, stable crack growth can be observed if the crack tip conditions are held steady and the microstructure of the material is uniform.

SCC initiation and growth are classified as phenomena that take place at constant stress or stress intensity, respectively. The addition of cyclically controlled loading or straining, or even monotonic load or strain changes over relatively long periods of time such as a few weeks can cause an accelerated response that is classified as stress corrosion fatigue or corrosion fatigue **[11]**. Thus, SCC measurements, whether it be initiation or growth, are normally performed under constant stress or stress intensity conditions, respectively.

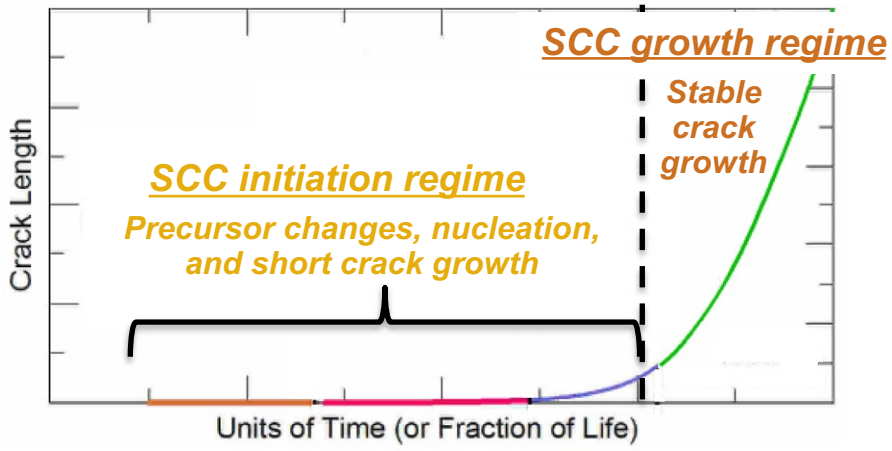

Figure 1. SCC as a multi-step process.

This page is intentionally left blank.

3. SCC GROWTH RATE MEASUREMENT TESTING APPROACH

3.1 Overview of SCC Testing

The goal of the PNNL CISCC testing effort is to produce quantitative stress corrosion crack growth data through in-situ measurement of cracking in instrumented, well controlled environments. As was discussed in the FY19 report **[4]**, crack length versus time data at constant load or stress intensity are acquired to obtain these quantitative measurements. In-situ measurement of crack length provides two distinct advantages over cook-and-look methods where cracking is determined in post-test observations. By revealing the moment-by-moment cracking response, it is possible to:

- Show whether crack growth is steady with time, decreases with time, or accelerates. This is potentially very important because at least one prior study in the literature where in-situ measurement of crack length has been used in deliquescent humid air tests has shown a decreasing crack growth rate with time **[8]**. Methods where post-test examination are used to determine crack length will not capture this behavior unless tests are run for a very long period of time and thus cannot show whether crack growth response is steady, increasing, or decreasing with time.
- Show the crack growth response under different testing conditions with a single specimen. A high resolution in-situ crack length measurement system will be able to time-efficiently show differences in cracking response for changes in environment such as test temperature, salt composition, salt content, and stress intensity. Another key advantage is the *on-the-fly* change in which *only* a single change (e.g., temperature or environment) is made as the crack is actively growing and monitored. This has been repeatedly shown to provide a much more definitive insight into the effects of changes compared to separate specimens/tests.

Another key capability for SCC testing is an ability to actively manage the cracking behavior of the specimen during an SCC test. This is often referred to as “actively managing a test”, and it encompasses a general testing approach where a crack tip geometry and crack tip location in the microstructure are optimized for SCC growth. This perhaps sounds as if the specimen is put into a condition where it is artificially more susceptible to SCC than in a real world environment. However, a better way to consider this is that a real world component will be exposed to a variety of environments, and at the same time, a wide spectrum of the component material microstructure will be exposed to the environment. From a stochastic perspective, there will always be a small but non-zero probability of a portion of a real world component with susceptible microstructure being exposed to optimal conditions to produce stress corrosion cracking. An actively managed test aims to assess that type of real world condition where cracks are most likely to first occur.

A further issue is the relevance of an artificial fatigue precrack, which is used in laboratory growth rate tests but may not behave similar to a crack that has initiated and always grown as an SCC crack. Continuous crack monitoring allows the crack to be transitioned from fatigue to SCC and has been widely shown to be a key element in obtaining relevant and reproducible SCC growth rates.

3.2 In-Situ Crack Length Measurement

PNNL uses the direct current potential drop (DCPD) technique to perform in situ observation of crack initiation and crack growth. A sketch of the DCPD wiring arrangement configured for a single compact tension (CT) crack growth rate specimen is shown in Figure 2. As with all DCPD measurement systems, a constant current runs through a specimen, and the voltage across the crack plane is measured and converted into a crack length by means of a finite element model confirmed by experimental confirmation. The use of an additional voltage probe that is not sensitive to crack advance is an option that exists and is often needed in cases where significant resistivity evolution occurs in the specimen material at the test temperature. This reference DCPD voltage measurement can also compensate for

variability in test temperature. The use of a reference DCPD voltage probe does come at the expense of somewhat increased crack length noise levels. An example of an in-situ crack length versus time plot of an ongoing CISCC test at PNNL is provided in Figure 3. This is a two-specimen test, so there are two crack length versus time traces on the plot. In this example, it can be seen that the response of the specimens started off at a crack growth rate (CGR) that is approximately 3x higher than the terminal CGR, showing that for short term tests, in-situ measurement can provide a better estimate of long term cracking response than a cook-and-look test.

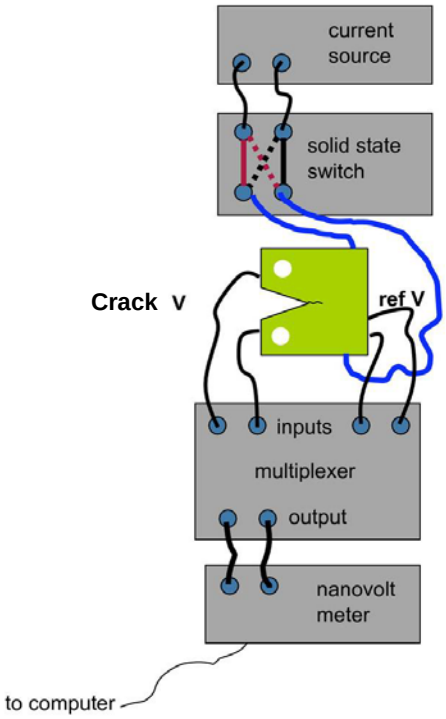

Figure 2. Sketch of DCPD data acquisition system and voltage probe locations for CGR testing of CT specimens.

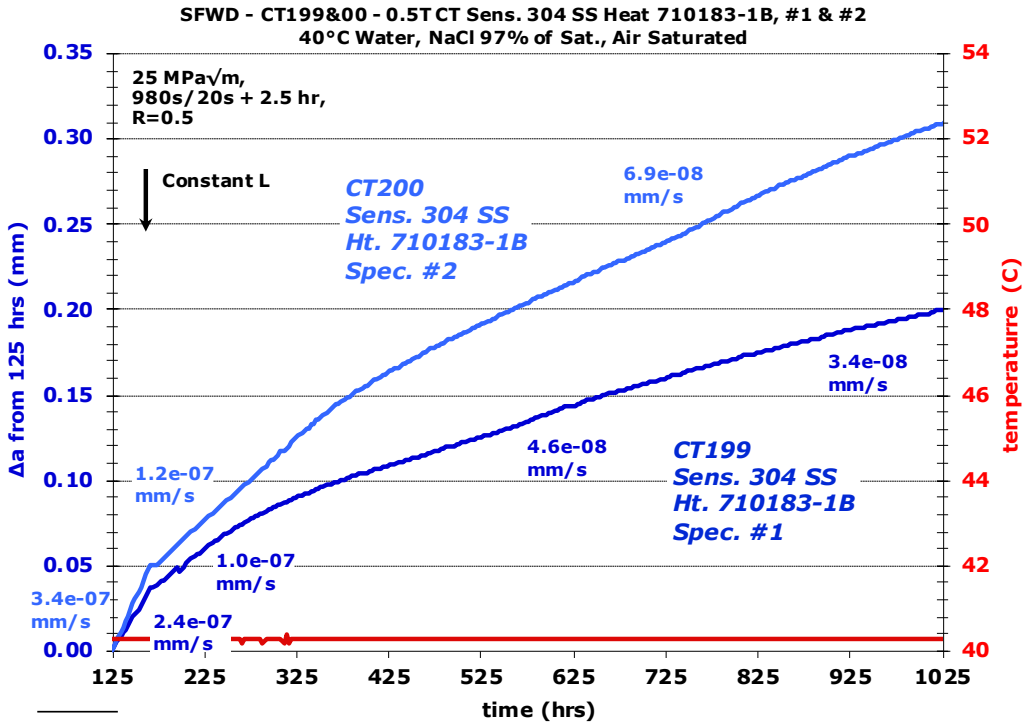

Figure 3. CISCCGR test of sensitized 304 SS in 40°C water saturated with NaCl and air.

In order to obtain useful in-situ crack growth rate data, a sufficient level of crack length resolution is needed, and this is dependent on the desired minimum measurable crack growth rate and the desired length of time needed for the measurement. For instance, if the minimum desired measurable crack growth rate is $1x10^{-9}$ mm/s over a period of 500 hours, this means being able to resolve a 2 µm crack length increase over that period of time. From a statistics-based approach, it might be concluded that crack length noise levels need to be 5-10x lower than the required resolution, but in fact, determination of a slope line to obtain a crack growth rate measurement can often be accomplished with noise levels that are the same or somewhat higher than the amount of crack advance such as shown Figure 4 for an LWR SCC test conducted at PNNL **[10]**. As noise levels increase, the required observation time needs to increase. Some of the CRIEPI CISCC growth rate data like that shown in Figure 5 **[8]** is an example of a crack growth rate that was extracted from relatively noisy in-situ crack length data by waiting a sufficiently long period of time, although the confidence in such a result is lower. In all cases, it is also important for the average trend in the data to be sufficiently steady. This often requires a very stable test environment.

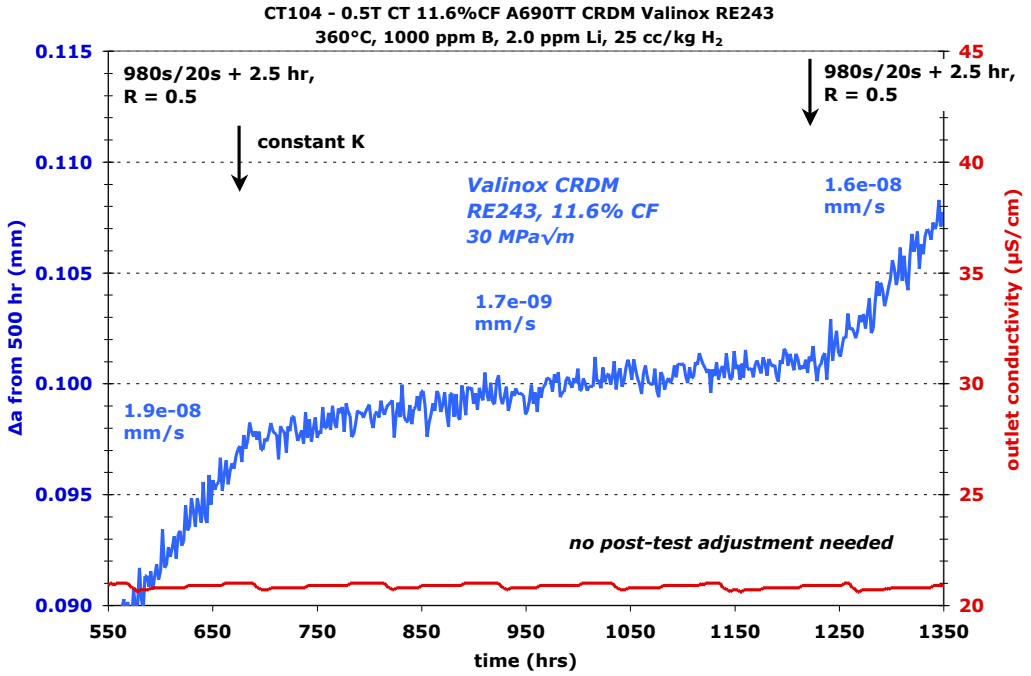

Figure 4. SCC growth response of a 12% cold forged Alloy 690 material that exhibited low-to-moderate SCC growth resistance [10].

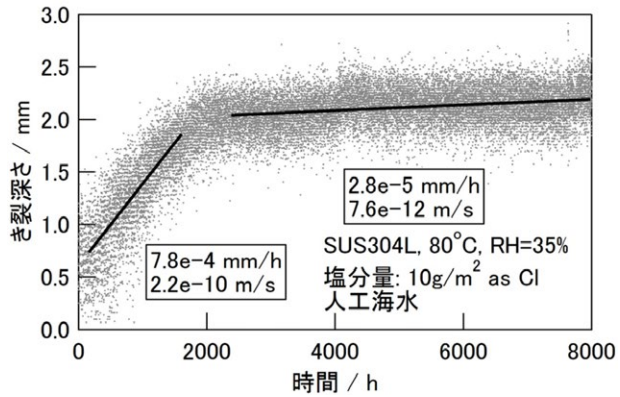

Figure 5. DCPD-based in situ crack length measurement during constant load as performed by CRIEPI during CISCC studies [8].

When the resolution is sufficiently good to allow rapid assessment of crack length, then it becomes possible to assess multiple environmental conditions on a single specimen. Typical examples of this approach for crack growth rate testing are assessing SCCGR as a function of test temperature, water chemistry (salt concentration, pH, dissolved oxygen, etc.) and stress intensity factor, with an example of the latter shown in Figure 6 for a specimen undergoing SCC testing in a simulated LWR cooling water environment **[10]**. Being able to measure environmental effects on a single specimen provides substantial economy of time and effort. Tests such as these can be run with little involvement from lab staff other than to maintain steady test system operation. Making the measurements *on-the-fly* on a single specimen adds confidence that the observed trend is real and reproducible.

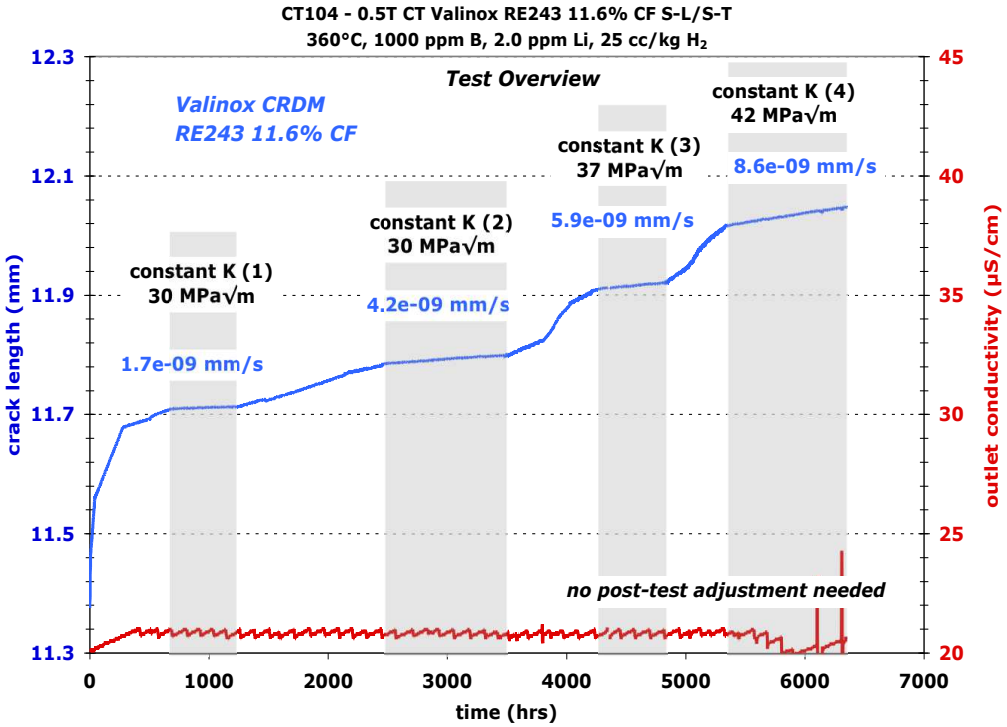

Figure 6. SCCGR test of a 12% cold forged Alloy 690 material in simulated LWR reactor cooling water [10].

3.3 Control of Specimen Load

As will be evident in the next section, there is substantial value in having full control specimen load during a test. In particular, the ability to apply cyclic loading steps is highly valuable for two basic reasons. First is that it is needed to advance the crack to new regions/microstructures of a specimen so that multiple SCC evaluations in different areas are obtained to gain confidence in the SCC growth rate measurements. Second is that cyclic loading provides the ability to attempt to "transition" a crack to a condition where it is susceptible to SCC. This will be explained in Section 3.4.

3.4 SCC Crack Growth Rate Testing

An important aspect of SCCGR testing is management of specimen response during a test. The goal of test management is to allow the specimen to have sufficient opportunity to exhibit SCC growth for the given environment. For a variety of reasons, an existing crack may initially be resistant to growth in an SCC environment. In cases such as this, management of the crack is needed to evaluate the susceptibility to SCC growth. Some examples are provided here.

For some materials in some environments, SCC growth occurs much more rapidly on grain boundaries than transgranularly through the matrix. For those materials, it is important to make sure that the crack has an opportunity to find grain boundaries, given that the fatigue precrack is transgranular and cyclically hardened. This is accomplished through test management as described here. Cracks in an SCC growth specimen are always started from a fatigue precrack grown from the machined notch in the specimen. Fatigue precracks are typically transgranular in nature, and if the particular material is only susceptible to intergranular SCC (IGSCC) in the environment, then the transgranular precrack needs to be given a chance to convert to an intergranular crack. A transgranular crack intersects grain boundaries at multiple locations along the crack front, and for materials and environments where IGSCC susceptibility is high, a

transgranular crack can readily develop into an intergranular crack with minimal test management. However, for materials that are resistant to transgranular SCC (TGSCC) and have only a mild or moderate degree of IGSCC susceptibility, management of the crack may be required to obtain IGSCC growth. This is accomplished through a series of more and more gentle cyclic loading steps as shown for example in Figure 7. In each step, the crack advances more slowly so that the driving force for TG cracking through the grains is reduced, giving the crack a chance to shift onto grain boundaries. An important issue with this approach is that the slower rate of advance also means that fewer grain boundaries are intersected versus time. The cyclic loading conditions that give the greatest amount of crack advance while still favoring advance along grain boundaries are desired. For large grained materials such as fusion welds, finding the ideal cyclic loading conditions can be a challenge if the material is only mildly susceptible to IGSCC. Evaluating highly SCC resistant materials is always a challenge and can require more than 5000 hours of testing before a satisfactory SCC assessment has been accomplished on a particular specimen.

CISCC testing of stainless steels at PNNL indicates that these challenges, which have been widely observed in LWR tests, also apply to CISCC. For example, TGSCC advance will not automatically occur from a transgranular precrack when a constant load is applied, and this has been a common historical approach. Instead, the crack has to be transitioned to an SCC condition in very much the same way that transitioning steps are conducted for materials with low to moderate IGSCC susceptibility. In addition, there are indications that crack tip blunting can occur under some conditions during CISCC testing, and this can inhibit sustained crack growth because the stress intensity factor is substantially reduced as the crack blunts. A similar tendency for blunting is sometimes seen for SCC of stainless steels in simulated nuclear reactor core cooling water. If a particular SCC testing condition does not drive SCC growth, the crack tip can blunt, and subsequent efforts to recreate a sharp crack tip require very aggressive cyclic loading conditions. Careful consideration of cracking response and application of appropriate load cycling steps are needed to effectively evaluate SCC response.

Another aspect of specimen management is maximizing the uniformity of SCC growth along the width of a crack. SCC behavior can vary across the crack front due to many factors such as local chemistry, grain boundary character and local orientation, internal stress, and the degree of local strain. In some cases, regions of the crack front can be pinned, and the overall front become very uneven. This is especially prevalent for IGSCC in nickel-base weld metals. It is important to periodically take steps to unpin and straighten the crack front and, in the process, assess the extent of unevenness. Typically, this involves low frequency cyclic loading (corrosion fatigue) that usually drives crack advance along the entire crack front. The aggressiveness of the load cycling depends on the degree of straightening that is thought to be needed, and the desire to minimize the subsequent transition to SCC. Crack front straightening is characterized by an elevated initial growth rate decreasing to a steady state growth rate over time. Once the crack is thought to have been straightened, loading conditions are transitioned back to constant stress intensity SCC conditions.

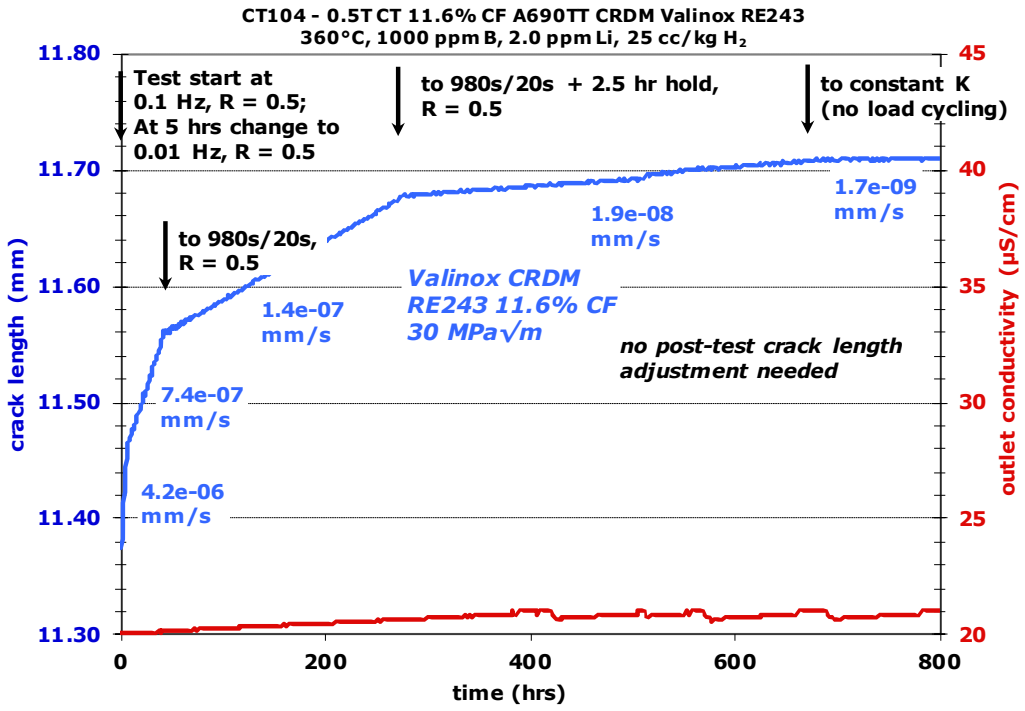

Figure 7. Initial transitioning attempt for an SCCGR test of a 12% cold forged Alloy 690 material in simulated LWR reactor cooling water [10].

This page is intentionally left blank.

4. REVIEW OF PNNL CISCC TEST PLAN

4.1 Review of Testing Strategy

As discussed briefly earlier, the PNNL approach is divided into multiple steps that each contribute to a foundational understand of CISCC response and provide quantitative crack growth rate data. An important element of this test plan is first evaluating CISCC in brine solutions. A brine solution provides a stable, well defined water chemistry to which CISCC response under deliquescent conditions can be compared. Inherent in this approach is that 1) the water chemistry is very well defined and stable, 2) the water chemistry is easily changed during a given test, and 3) the defined bulk chemistry provides excellent linkage to extensive SCC data and to the CISCC response under deliquescent conditions. Since humid air deliquescent salt solutions are salt saturated, testing in brine solutions is being conducted at the saturation level. There are three overall phases of the test plan.

Phase 1: CISCC testing will begin in saturated brine solutions. The first phase of the testing involves fabricating test systems, assessing test system performance, making any needed modifications to the test systems, and performing a calibration of DCPD-estimated crack length in saturated salt solutions. Since the DCPD crack length measurement method relies on measuring a resistance (via a voltage measurement using a fixed applied current), the use of brine solutions that have a 10^4 higher conductivity compared to our previous experience performing LWR SCC testing may affect the DCPD calibration because the brine solution in the crack and around the specimen can act as a current conducting medium. A series of tests will be performed to establish this calibration for both CT specimens and 4PB specimens.

Phase 2: Establish CISCC growth response in brine solutions. Testing in an aqueous solution has the advantage of providing a consistent, known bulk water chemistry. While the crack tip chemistry is expected to differ from the bulk solution chemistry, aqueous testing will provide a stronger, more consistent link between bulk solution chemistry and the crack tip chemistry than when testing salt loaded specimens in humid air. This will allow for clearer quantification of CISCC response under varying environmental conditions such as stress intensity factor, temperature, salt concentration, salt composition (including inhibitors), pH, dissolved oxygen, and material condition. Tests in saturated brine solutions will be conducted using both CT specimens and 4PB specimens to further confirm that a 4PB test can serve for measuring SCC growth. Phase 1 and Phase 2 will overlap in that some of the data obtained as part of the DCPD calibration are expected to be applicable toward Phase 2 testing. Phase 1 and Phase 2 combined are expected to require approximately 2-3 years to complete starting from FY19. Compared to the FY19 test plan discussion, this time frame has been extended based on research progress and test results obtained in FY20. The brine solution CISCC test results will serve as a baseline for comparison to humid air tests, and thus have high value. During this time, the humid air circulation system, potentially with salt fog capability, will be designed and constructed.

Phase 3: Humid air tests are planned to assess many if not all of the same dependencies measured in brine solutions. A stronger emphasis on material condition and heat-to-heat variability will be incorporated into this test matrix. Because of potential challenges with deliquescent solutions ineffectively migrating down a crack, test response may be more varied and require more tests and/or longer test times to effectively evaluate response and demonstrate reproducibility. Humid air testing will eventually include assessing diurnal cycles. Total time to complete all currently planned tests is 3-4 years.

4.2 Review of Material Condition

Another important factor to consider in designing a test matrix is material condition. Deformation, especially cold deformation, has been shown to increase SCC susceptibility during LWR SCC testing of stainless steels, Ni-base alloys, and low alloy steels. One simple mechanism postulated for this is that a stronger material creates a smaller plastic zone size and therefore a steeper stress/strain gradient near the

crack tip. Thus, per unit of crack advances, more strain redistribution occurs near the crack tip, which means higher crack tip strain rate. Such a mechanism could readily translate over to CISCC response. Deformation and/or higher strength in dry cask storage system (DCSS) containers can be caused by a variety of events, including non-optimal material processing conditions at the alloy fabricator, bending of the plate to make the cylindrical casks, material or component handling impacts, and local shrinkage strains in the vicinity of the heat affected zone along the welds joining the plate pieces together. In general, all these events are unavoidable during fabrication and handling of a large number of components and, as a result, the baseline material for a DCSS CISCC testing program should incorporate some cold work, although experts may disagree on the most relevant level. SCC initiation and growth in LWR pressure boundary components has almost always been associated with deformation of a material from the same factors described for DCSS containers, and the currently estimated 75 percentile level of deformation of Alloy 690 pressure boundary structures is about 12% **[7]**. Residual deformation levels above 20% are observed in various welded austenitic components, and 8% residual deformation is observed in mockups from incomplete annealing. Thus, many LWR SCC pressure boundary material testing programs have included cold worked material in their assessments.

If SCC is likely to occur first and cracks grow faster in regions of higher strength, then there is a reasonable argument for cold worked material to serve as the primary material being tested, or at a minimum, it should be a key part of the material conditions that are evaluated. PNNL has taken this approach and is including cold worked material in its test matrix. PNNL had originally planned to perform nearly all testing on cold worked material, but high SCC growth rates observed during early CISCC testing of non-cold worked material in FY20 indicate that CISCC of non-cold worked stainless steel will also need to be widely assessed.

When studying cold worked materials, the deformation level and deformation mode must be defined. For DCSS some of the likely strains can be estimated. Bending strains caused by rolling 15 mm thick sheet into an ~2.5 m diameter cylindrical shape to make a DCSS is <1% at the outer surface, while strains in the base metal in the vicinity of a weld can exceed 10% deformation. Other potential sources of deformation are more difficult to quantify, in particular component and cask handling and impact strains. For this test plan, a tentative decision has been made to select 10% strain as the deformation level in cold worked materials. Since typical deformation in the containers is tensile deformation (due to plate forming and weld shrinkage strains), the 10% cold work (CW) level will be achieved using tensile straining methods.

Another important material factor is the heat affected zone (HAZ) around welds. An important hallmark of a weld HAZ in normal grades of (moderate carbon level) stainless steel is sensitization. A variety of microstructure changes can be induced during welding, and for SCC response, an important microstructure change is a reduction in chromium content along the grain boundaries (sensitization). This can result in higher IGSCC susceptibility because chromium aids in producing a stable passive layer. It is important to simulate and assess weld HAZ susceptibility as part of the testing program.

Another material factor that will be addressed in the testing effort is heat-to-heat variability. Drawing again on LWR SCC experience, it has been observed that some materials exhibit much higher susceptibility than others **[5-7]**. Whether or not the microstructural factors that affect the variability can be determined, it is necessary to test multiple heats to quantify this variability as best as possible so that service response can be adequately estimated. An extensive characterization of heat-to-heat SCCGR variability requires testing a large number of heats, likely well beyond what has been anticipated by the DCSS CISCC measurement community. For SCCGR measurements of next generation Ni-base alloys for PWR pressure boundary materials, PNNL tested more than 10 heats of Alloy 690 **[10]**, and for the EPRI Alloy 690 PWSCC crack growth rate database that was assembled from multiple labs across the world, 22 heats were tested **[7]**. For the PNNL PWR SCCGR research program, only one heat was tested extensively, but several others were tested semi-extensively, and additional heats were tested at key environmental conditions. The current test plan will perform extensive testing on three heats of material - two heats of 304L and one heat of 316L.

4.3 4-Point Bend Specimen Usage

4.3.1 Specimen Design

As was covered in detail in the FY19 report, PNNL has put extensive effort into development of a 4PB test specimen and fixturing **[12]**. This activity was undertaken for LWR SCC testing needs, but the specimen and fixturing are fully suited for evaluation of CISCC in deliquescent humid air conditions. Examples of the test specimen geometry in Figure 8 and Figure 9 show that it can be used for typical crack growth rate testing (Figure 8) as well as for assessing crack growth from short cracks growing from a flat surface (Figure 9). The short crack geometry is ideally suited to CISCC testing in deliquescent humid air conditions. All efforts needed to perform in-situ measurement of crack growth on these specimens has been completed, and usage of this specimen geometry can begin at any time.

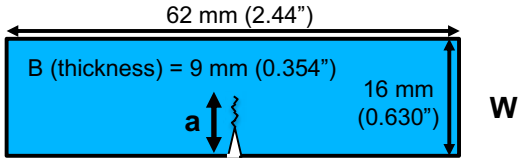

Figure 8. 4PB crack growth rate specimen.

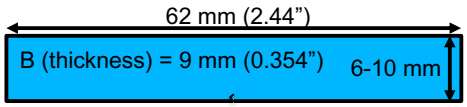

Figure 9. 4PB crack initiation and shallow crack growth specimen.

4.3.2 Test Fixture Design

As covered in the FY19 report, extensive efforts have also gone into designing and producing fixtures for conducting 4PB SCC tests. The PNNL 4PB test method has all of the same capabilities as CT specimen crack growth testing at PNNL. Key attributes are as follows:

- The ability to actively load the specimen so that load can be adjusted on-the-fly and also to allow for fatigue cycling to manage the crack front shape, transition to SCC behavior, advance the crack to sample multiple regions of a specimen, and maintain constant stress intensity factor as the crack grows.
- The ability to be able to perform in-situ measurement of crack length by DCPD.
- The ability to link multiple fixtures in series in such a way that the load is transmitted to all specimens. The obvious advantage is being able to test multiple specimens in a single environmental chamber. This is important for evaluating the crack growth response for many heats, material conditions and stress intensity factors.

A rendering of the fixturing that successfully incorporates all these features is presented in Figure 10, which shows a two-unit assembly (although many more can be accommodated). The fixture is comprised of multiple pieces: load pads, ceramic insulators, an “inner traveler”, a spacer shim, a load transfer pin, and the preload screw that aids in mounting the specimen in the fixture and provides the option for maintaining load on a specimen while applying any surface treatments of interest. Examples of actual fixtures with test specimens are presented in Figure 11. The image on the left shows a PNNL 4PB fixture

with a crack growth rate specimen, and the middle image shows a fixture with a crack initiation or shallow crack growth specimen. A variety of LWR SCC tests have been conducted using this fixturing. A simple proof test of nine specimens in a single string such as shown in the rendering on the right side of Figure 11 has also been conducted. While this test method and fixturing were developed for a completely different programmatic need, it has virtually all the features needed to perform high precision, quantitative CISCC growth rate and initiation testing in support of U.S. Nuclear Regulatory Commission (NRC) needs.

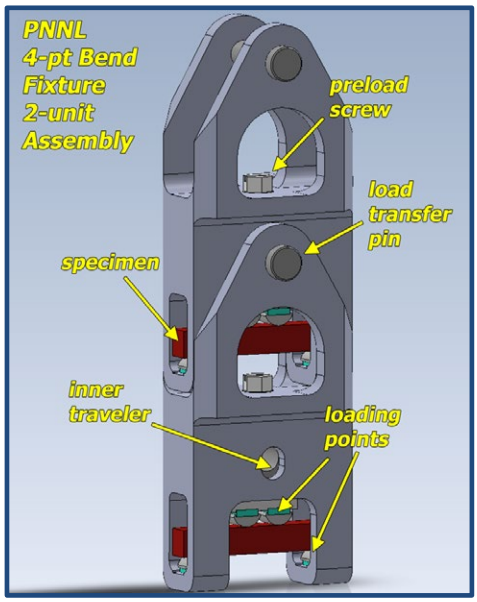

Figure 10. Rendering of a two-unit fixture assembly showing key features.

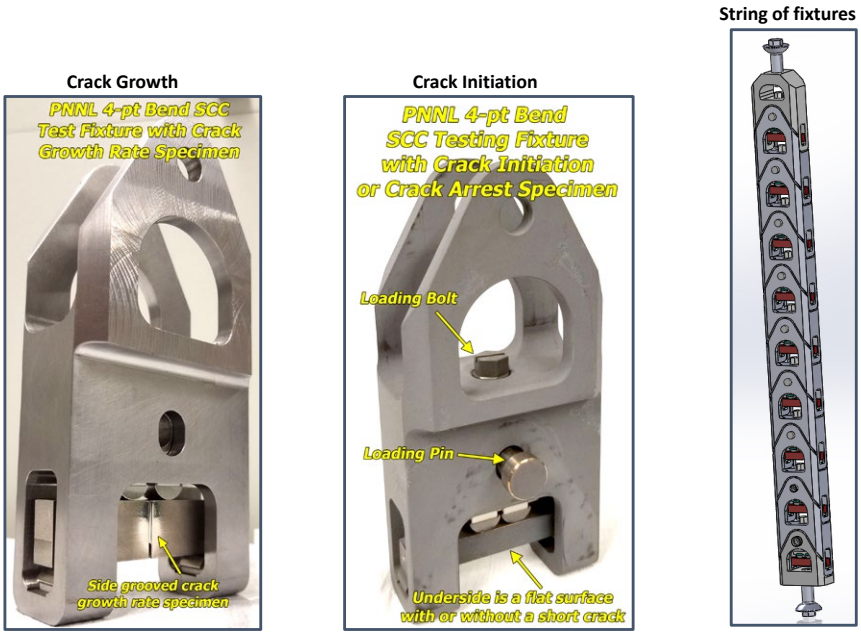

Figure 11. Two images of actual fixtures and a rendering of a string of nine specimens.

5. CISCC TEST SYSTEM DEVELOPMENT

5.1 Overview

In FY19, a dedicated lab space shown in Figure 12 was set aside for the CISCC test systems. A photo of all four test systems is shown in Figure 13. As of the writing of this report, all four test systems are fully constructed, with CISCC1 and CISCC2 being used for CISCC tests while CISCC3 and CISCC4 are undergoing thorough shakedown evaluation. These systems are currently set up for testing in immersed conditions. Six specimens can be tested simultaneously in each test system with all specimens instrumented for in-situ measurement of crack length by the DCPD technique. Load is actively controlled based on crack length with a servoelectric load control system that can achieve loading frequencies up to 3 Hz, which is well beyond what is needed in this CISCC project. Temperature is actively controlled with the ability to run at temperatures from ~30°C to 80°C. The entire loop runs at the test temperature. Since SCC crack growth is being readily observed in non-cold worked 304L SS in NaCl at 40°C at PNNL, we see no need to conduct tests in boiling solutions, and our expectation is that most testing will be conducted at 40°C or below, which corresponds to deliquescence that can routinely occur on DCSS stainless steel containers. Water is continually filtered down to 1 µm and is air saturated in a glass column. All pertinent data is recorded by custom software that also can automatically control incremental changes in cyclic loading conditions and applied stress intensity factor as the crack advances. All fixturing needed to conduct CT specimen and 4PB crack growth tests has been fabricated.

Figure 12. PNNL CISCC testing laboratory.

Figure 13. All four PNNL CISCC test systems. CISCC3 and CISCC4 were partially constructed at the time of this photo but are now complete.

5.2 Construction of CISCC3 and CISCC4

Construction of CISCC3 and CISCC4 was uneventful and completed on schedule. These systems are nearly identical to CISCC1 and CISCC2 with all four test systems having the improvements described in Section 5.3. The only differences between the two new systems and the two older systems are as follows:

- The heater systems on CISCC3 and CISCC4 have more heater controllers and thus have the ability to separately control more heater zones. We currently do not need the capability of these heater systems, but it may be needed for testing in humid air. CISCC1 and CISCC2 can be upgraded at a later date if needed.
- The load frames on CISCC3 and CISCC4 are taller. As with the upgraded heater systems, this was a future-proofing move that can allow for a taller environmental chamber to be used that can hold more specimens.

5.3 Test System Modifications

5.3.1 Production of Air Saturated Water

A deliquescent solution in humid air will always be air-saturated, and thus our intent for tests in saturated brine solutions is to use air saturated water. A fine dispersion of air bubbles in water is an effective means to aerate water, and stone fritters/bubblers are often used for this purpose. PNNL LWR SCC test systems that utilize water with low ionic content are outfitted with stone bubblers for the purpose of dissolving a variety of gases into the test system water. During early usage of CISCC1 and CISCC2 it was found that a traditional stone bubbler rapidly clogged in saturated and near-saturated brine solutions. The brine solution infiltrates the stone bubbler while at the same time, the air leaving the bubbler dries the solution touching the bubbler, leading to clogging. Other aeration methods were explored to eliminate the clogging. As part of this effort, the process of aerating the water was moved from the environmental chamber to a separate glass column and a pump was installed to circulate water between the column and the environmental chamber. Two methods of aeration were evaluated in pure water. For both methods, the column is partially filled with water, and the unfilled portion is continually fed with fresh house-air. A Swan dissolved oxygen (DO) sensor with resolution of 1 ppb in pure water was used for evaluations. Saturation levels of DO in water are readily calculated from Henry's law using calibration data available from a variety of sources **[13]**. The sensor probe was positioned in the environmental chamber for observations.

The first method evaluated is a waterfall method where water is fed to the top of the capped glass column and allowed to run down the inside of the air-filled portion of the column. The thin layer of water running down the inside column has high surface area that enables the water to become air saturated. A jet bubbling method, where a water nozzle is placed just above the waterline in the column and adjusted to point towards the pool of water in the column, was also evaluated. A high speed flow of water from the nozzle creates a high density of bubbles in the column. The dissolved oxygen levels obtained by the above two methods were compared to stone bubblers in the column and EVC. Measurements with no active aeration were also performed to provide another point of reference for the effectiveness of the different methods.

The data in Figure 14 show the waterfall and jet methods are as effective as a traditional stone bubbler. Comparison to saturated DO values in pure water taken from a variety of field data **[13]** indicate that these methods can fully saturate the water with oxygen. Measurements with no active aeration method were erratic and show the necessity of aeration. Trials of the waterjet method using a nearly saturated NaCl solution revealed that excessive caking of the water column walls above the waterline occur from water running down the column, so the jet bubbling method was selected for CISCC testing.

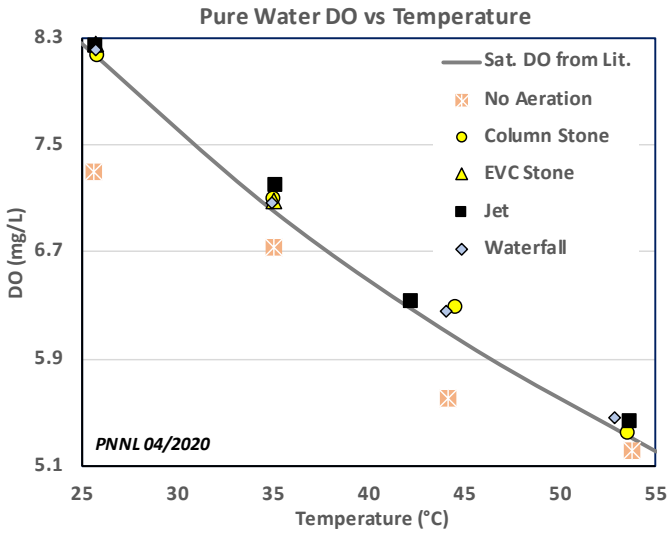

Figure 14. Dissolved oxygen content in pure water as produced by several methods. Henry's Law fit to a variety of field data [13] is also shown.

5.3.2 Reduction of Crack Length Measurement Variability and Noise Levels

The ability to measure crack extension in the micrometer range requires being able to measure nanovolt changes in the DCPD voltage signal in the crack. For a half size (0.5T) compact tension specimen with a crack that is approximately half way through the specimen and with an applied DCPD current to produce a crack voltage of ~150 µV, a 1 µm increase in crack length corresponds to an approximate 15 nV DCPD signal increase for the DCPD configuration used by PNNL. Thus, a voltage resolution of 10s of nanovolts is needed to efficiently measure low crack growth rates, in particular for crack growth rates below ~$5x10^{-9}$ mm/s. In addition, a steady DCPD signal requires a stable environment for a number of reasons. Temperature is one of the more important factors because the resistivity of metals is temperature dependent. A one degree centigrade change in temperature can lead to an ~100 nV change in the DCPD signal which would be equivalent to an ~7 µm shift in crack length. Thus, temperature fluctuations of +/- 0.5°C will induced large amounts of noise in the crack length data and may require very long observations times (several months or more) to make in-situ crack growth rate measurements of ≤$1x10^{-8}$ mm/s (~300 µm/year). Salt concentration can affect the water conductivity and hence the voltage reading during a test, although this has yet to be quantitively evaluated.

Other aspects of the lab environment may also contribute to large crack length noise levels, in particular, background electromagnetic noise levels appear to strongly affect DCPD noise in highly conductive solutions. Ground noise and ground loops can also introduce DCPD noise. Through a combination of basic noise reduction techniques and trial-and-error electronics configurations, DCPD noise levels have been reduced by an order of magnitude compared to our initial DCPD system configuration. Provided that the test environment is held sufficiently stable, it is readily possible to measure crack growth rates as low as $1x10^{-9}$ mm/s that is needed to assess low growth rate behavior of stainless steels.

5.3.3 Introduction of Water Filtration

To provide more consistent water chemistry, a 1 µm high flow rate filter was added to the water recirculation loop. Early observations of used filters revealed substantial pickup of iron-based corrosion product in test systems containing fixturing made from less corrosion resistant materials. Observations of used filters from test systems using all corrosion resistant fixture and load line materials have yet to be performed, but it is expected that the amount of corrosion product in the filters will be much less.

This page is intentionally left blank.

6. MATERIALS SELECTION, CHARACTERIZATION, AND PREPARATION

6.1 Overview

A high degree of confidence that the SCC response observed in this testing task is applicable to service structures relies in part on the materials that are tested. A key factor in selecting materials is understanding that variability in material properties, including SCC response **[10]**, occurs even within a specific alloy specification and that cracks in service structures are most likely to occur in cases where the particular heat of material used for that structure has greater SCC susceptibility. Alloy fabrication techniques have evolved over the last 50 years, mostly driven by the need to remain cost competitive. These new techniques, in particular continuous casting and rolling without further processing, can result in an alloy with less than optimal material microstructure, but the material will still meet the required specification in terms of composition, physical, and mechanical properties. An example of a commercial heat of continuous cast and rolled Alloy 600 plate from a well known alloy fabricator is provided in Figure 15. SCC initiation testing of this heat of material in simulated LWR core cooling water has revealed a tendency for SCC initiation to occur on the large grains shown in these images **[14, 15]**.

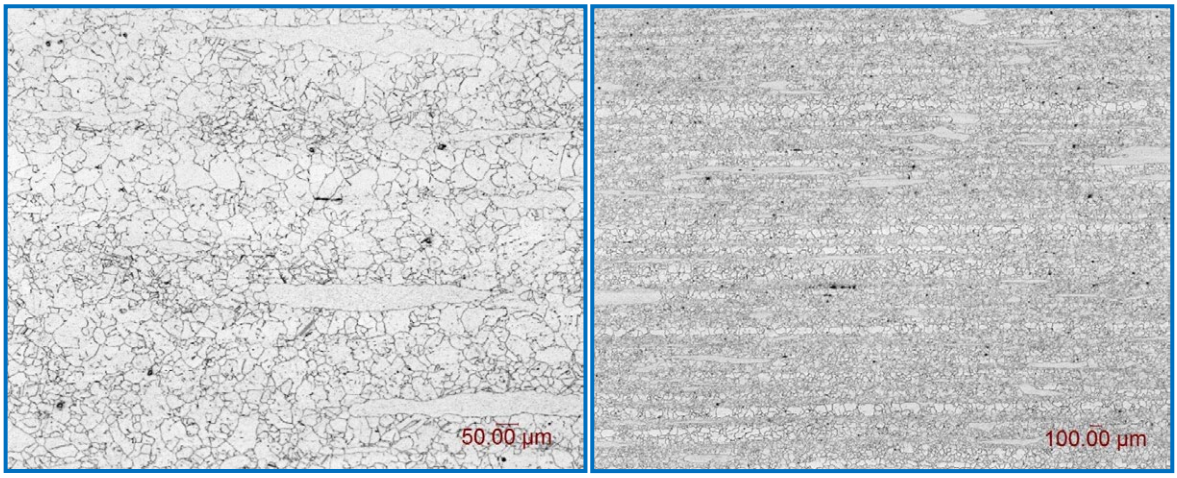

Figure 15. Inhomogeneity of grain size and carbide distribution in a commercial heat of continuously cast and rolled Alloy 600 plate [14].

With respect to CISCC response of 304/316, one factor that may affect cracking behavior is the strength of the material. For a given material, SCC susceptibility often scales with material strength. If there is a need to understand when the earliest SCC may occur in a service structure, testing should take place on materials with the highest strength. Strength can vary by a few different factors. Heat-to-heat variability is a common factor that leads to small variations in material composition and microstructure within the specification, e.g., grain size and solute content both influence yield strength. ASTM A240 **[16]** sets the specifications for 304/316 composition and properties in the USA, and for this specification, the minimum required yield strength (YS) for 304 and 304L is 205 and 170 MPa, respectively. There is no specification on the upper limit of the alloy strength. Thus, alloy vendors only ensure that their heats of material have a yield strength that exceeds the minimum value. As a result, 304/316 are almost always found with a YS that is above the minimum value. Among the available heats of 304L that were surveyed by PNNL for use in this CISCC testing task, the lowest strength was 220 MPa while the highest was 300 MPa. This range is quite wide with the highest YS being 76% more than the minimum specification.

Container vendors are not required to select low strength heats of material, making it virtually assured that some of their container stock is made from 304/316 stainless steel on the higher end of the strength spectrum. Thus, when conducting CISCC testing, at least one heat of the material of interest should have a strength that is on the high end of the available range.

Another factor affecting material strength is applied deformation. Deformation of stainless steels raises the material strength. Such deformation can be caused by a variety of events, including improper material processing by the alloy fabricator, bending of the plate to make the cylindrical containers, physical impacts associated with raw material or component handling, and local shrinkage strains in the vicinity of the seam weld. Most of these deformations are induced at room temperature and can be classified as "cold" deformed. In general, all these types of deformation events are unavoidable, and as a result, a DCSS CISCC testing program should include tests on materials with some level of deformation. Crack initiation and crack growth in LWR pressure boundary components has almost always been associated with deformation of a material from many of the same factors described for DCSS containers, and the currently postulated level of maximum possible deformation of pressure boundary structures is approximately 10-12% **[7]**. Thus, many LWR SCC pressure boundary material testing programs have included cold worked material in their assessments.

Three possible scenarios can be considered for selection of deformation level used for the baseline material condition of this testing task: 1) No cold work, 2) mild cold work, and 3) high cold work. Many LWR pressure boundary SCC cracks have been associated with unintended deformation, which is also expected in DCSS containers. Thus, exclusive use of *non*-cold worked material for a CISCC test program is unlikely to provide realistic service susceptibility estimates. The majority of the cold deformation present in the DCSS container material is expected to be at a lower level. For example, bending strains caused by rolling 15 mm thick sheet into an ~2.5 m diameter cylindrical shape to make a DCSS container is <1% at the outer surface. However, for other fabrication processes (welding, forming, and handling operations), isolated local regions of up to ~20% cold work are possible. For this test plan, a tentative decision has been made to follow the LWR SCC community and include materials with a mild level of 10% CW in the test plan. Since typical deformation in the containers is tensile deformation (due to plate forming and weld shrinkage strains), the 10% CW level will be achieved using tensile straining methods.

One other factor in selection of the 304L for this testing task was obtaining at least two heats of different compositions while staying within the composition specification. For this aspect, the primary difference in observed composition among surveyed heats was Molybdenum content. The ASTM standard for 304/304L composition does not specify a Mo content range, and typically low Mo content is used because it is relatively expensive. Mo is generally considered to improve corrosion resistance, but to obtain this benefit, additional austenite stabilizing elements must be added to the alloy to prevent a greater tendency for ferrite/martensite formation that is detrimental to corrosion resistance. This is the approach used to make 316/316L, but for 304/304L, no effort is made to adjust the content of austenite former elements when the Mo content is higher. This can lead to a material this is actually more susceptible to SCC **[17]**.

6.2 Selected Materials

Three task materials – two heats of 304L and one heat of 316L – were procured with their composition and selected properties shown in Table 1 and Table 2, respectively All materials were obtained in a mill annealed condition. Note that P304L1, P304L2, and P316L1 have been assigned as abbreviated names. P304L1 and P316L1 were produced by the same mill. The composition of the two 304L heats is nearly identical except that P304L1 has 0.41 Mo while P304L2 has 0.10 Mo. Mo content is not specified in the ASTM A240 specification with the intent that it is not a required constituent. Both of the Mo levels are low compared to the 316 SS specification of 2.0 Mo, but without an increase in Ni content to match the higher Mo content, P304L1 will have a greater tendency to form ferrite and martensite during deformation which will increase the work hardening rate **[18]**. Mo is also a solid solution strengthening

element in stainless steels **[18]**. Sandia National Laboratories (SNL) was informed of these product acquisitions and has acquired some of these same materials for their CISCC testing effort.

Table 1. Composition of the three heats of stainless steel purchased for PNNL CISCC testing.

			Elemental Composition (%)													
Material	**Heat/ID**	**Name**	**C**	**Co**	**Cr**	**Cu**	**Mn**	**Mo**	**N**	**Nb**	**Ni**	**P**	**S**	**Si**	**Ti**	**Fe**
304L	ASTM A240 Spec		<0.03	---	18-20	---	2.0	---	0.10	---	8-11	<0.045	<0.030	0.75	---	bal
304L	04E28VAA	P304L1	0.017	0.234	18.1	0.412	1.782	0.414	0.080	0.014	8.030	0.037	0.001	0.236	0.002	70.7
304L	SD41059	P304L2	0.019	0.210	18.2	0.335	1.630	0.100	0.073	0.010	8.155	0.028	0.008	0.385	0.003	70.8
316L	ASTM A240 Spec		<0.03	---	16-18	---	2.0	2-3	0.10	---	10-14	<0.045	<0.030	0.75	---	bal
316L	02D84WAB	P316L1	0.017	0.360	16.7	0.477	1.178	2.002	0.062	0.023	10.085	0.037	0.001	0.282	0.004	68.8

Table 2. Selected properties from the certified materials test report (CMTR) provided by the alloy vendor of the three heats of stainless steel purchased for PNNL CISCC testing.

Material	Heat	Name	YS 0.2% (MPa)	HRB	Grain Size No. (ASTM E112.13)	Avg. Grain Size (µm)
304L	04E28VAA	P304L1	292	81	6.7	35
304L	SD41059	P304L2	242	78	5.2	59
316L	02D84WAB	P316L1	270	81	6.5	38

The materials were purchased as 1.5” thick plate. The orientation of the tensile straining and test specimens relative to the plate dimensions and plate mill processing direction are provided in Figure 16. A plate material thicker than that used to make DCSS containers was required to allow compact tension specimens to be oriented so that crack growth occurs in the same direction as it would in a DCSS plate material. Microstructure in modern continuously cast and rolled plate stainless steel is commonly anisotropic in appearance **[19]** (typical examples shown below), so orientation of test specimens to obtain realistic crack growth directions through the microstructure is one step towards ensuring that observed CISCC response is as representative as possible.

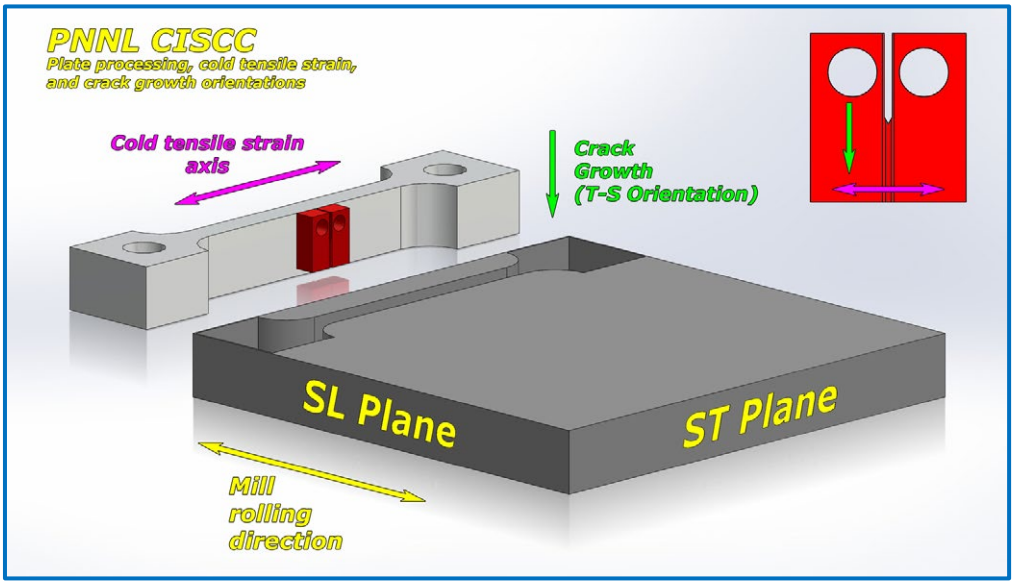

Figure 16. Orientation of tensile straining and compact tension specimens relative to the plate dimensions and mill plate processing direction of the PNNL CISCC testing materials.

6.3 Microstructure Observations

The specimens for optical microscopy were prepared by polishing to a 1 µm finish and then etched with 10% Oxalic acid at 7 V in 30 second increments until grain boundaries were readily identifiable. The higher resolution optical images shown here are from the mid-thickness of the plate which is where crack growth would occur in CT specimens cut from this plate due to the size of the specimen relative to the plate thickness. 4PB specimens are not as tall and can be taken from anywhere in the thickness. As will be shown, the microstructure in the mid-thickness of each heat was relatively uniform without any obvious issues, but some heats have variable microstructure from top to bottom of the plate as is common for continually cast and rolled (CCR) materials. There may be value in assessing CISCC response at the top and bottom of the plate using 4PB specimens because these microstructures may be representative of crack nucleation and growth from the surface of a DCSS container plate. Additional microstructure observations of actual DCSS plate material and these task materials will be needed to aid in making this decision.

6.3.1 Optically Observed Microstructure of Heat P304L1 (Heat 04E28V)

The microstructure is typical of CCR materials. Grain banding is present in both the ST (left image) and SL (right image) as shown in Figure 17. Note that despite the grain banding, the grain shape is relatively equiaxed. Twinning occurs with moderate frequency throughout the microstructure. A relatively minimal amount of grain size variability is present with average grain size of 35 µm taken from the certified materials test report (CMTR). This fine grain size is likely contributing to the high strength of this heat compared to heat P304L2 that has an average grain size of 59 µm. A modest amount of carbides and other precipitating or secondary phases are seen within grains (seen as small bright spots), occurring homogeneously throughout the sample. No obvious aggregation of carbides or secondary phases is seen at grain boundaries. A common characteristic of CCR materials is strong microstructural variability from top to bottom of the plate **[19]**. The microstructure of this test plate does show some variability from top to bottom of the plate as can be seen in Figure 18.

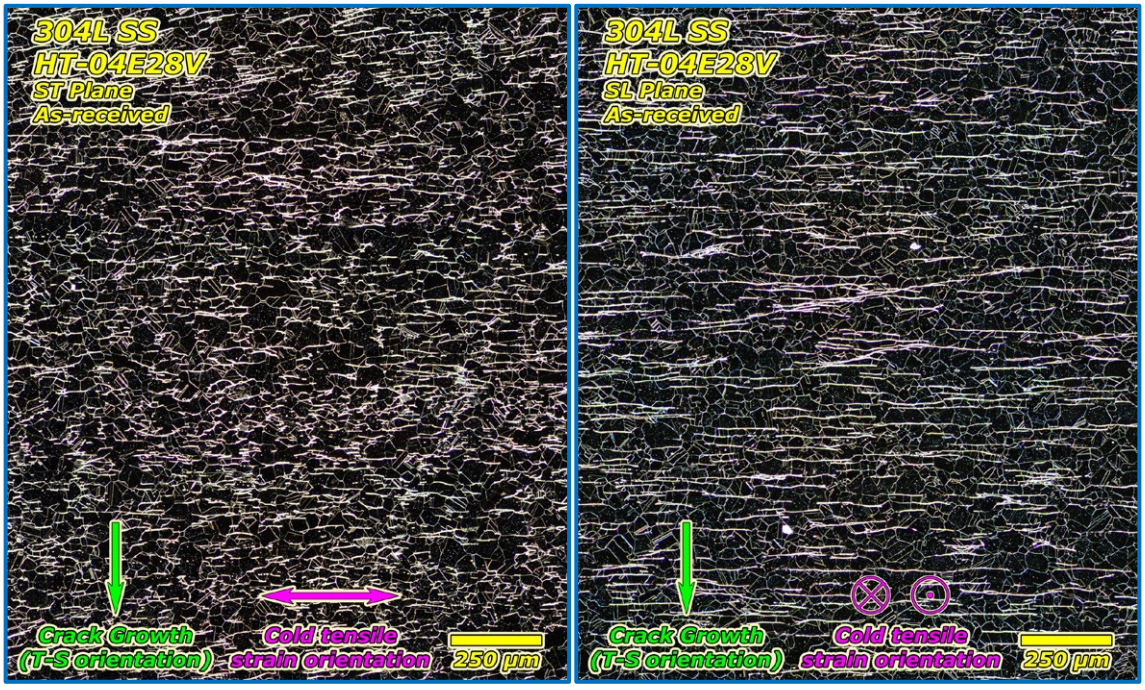

Figure 17. Dark field optical imaging of Heat P304L1 in the ST and SL plane relative to the plate shape and plate processing direction.

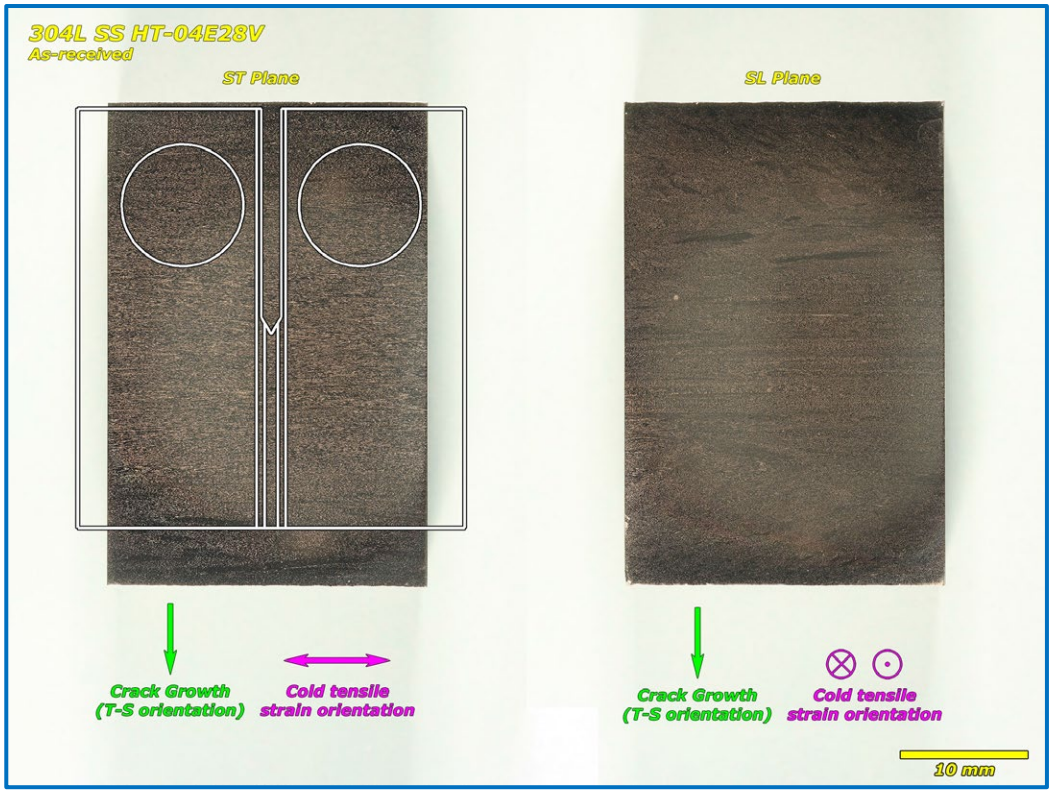

Figure 18. Low magnification bright field optical image of Heat P304L1 in the ST and SL plane showing microstructural variability from top to bottom of the plate.

6.3.2 Optically Observed Microstructure of Heat P304L2 (Heat SD41059)

The lack of any grain banding or carbide banding (Figure 19) makes this microstructure somewhat atypical of CCR materials. The average grain size of 59 µm is 1.7x larger than in Heat P304L1. Coarser carbides and other secondary or precipitating phases visible as bright dots occur throughout the microstructure, occasionally present along grain boundaries and in dense concentrations within individual grains. As can be seen in Figure 20, the microstructure from top to bottom of the plate is relatively uniform for this heat of material.

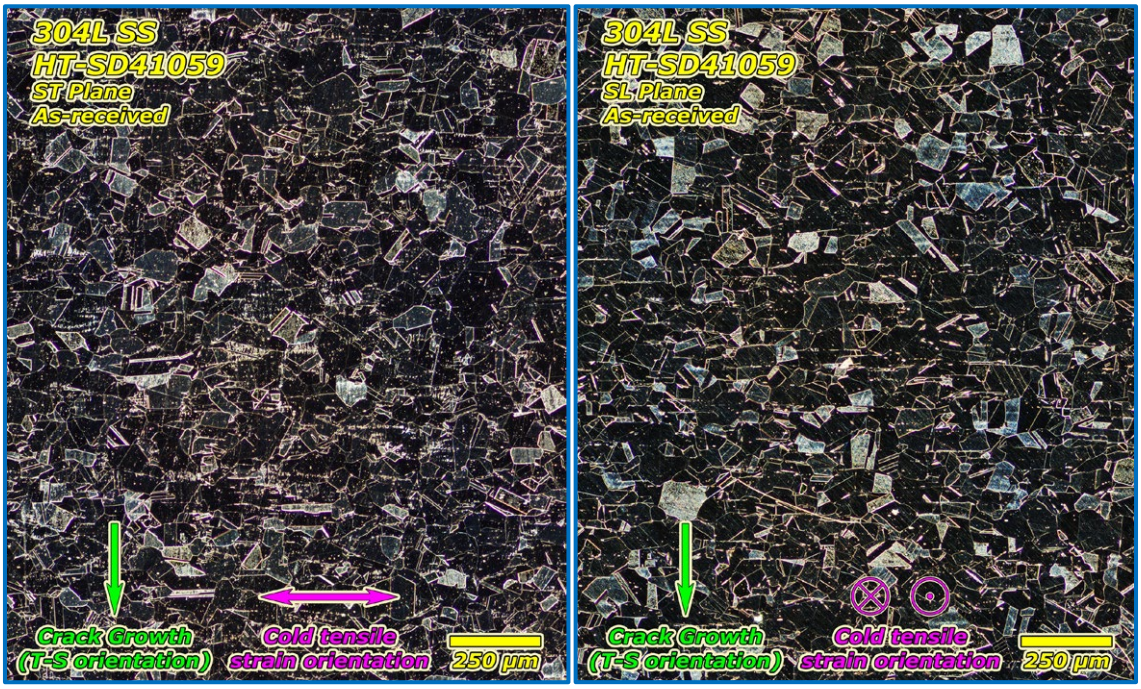

Figure 19. Dark field optical imaging of Heat P304L2 in the ST and SL plane relative to the plate shape and plate processing direction.

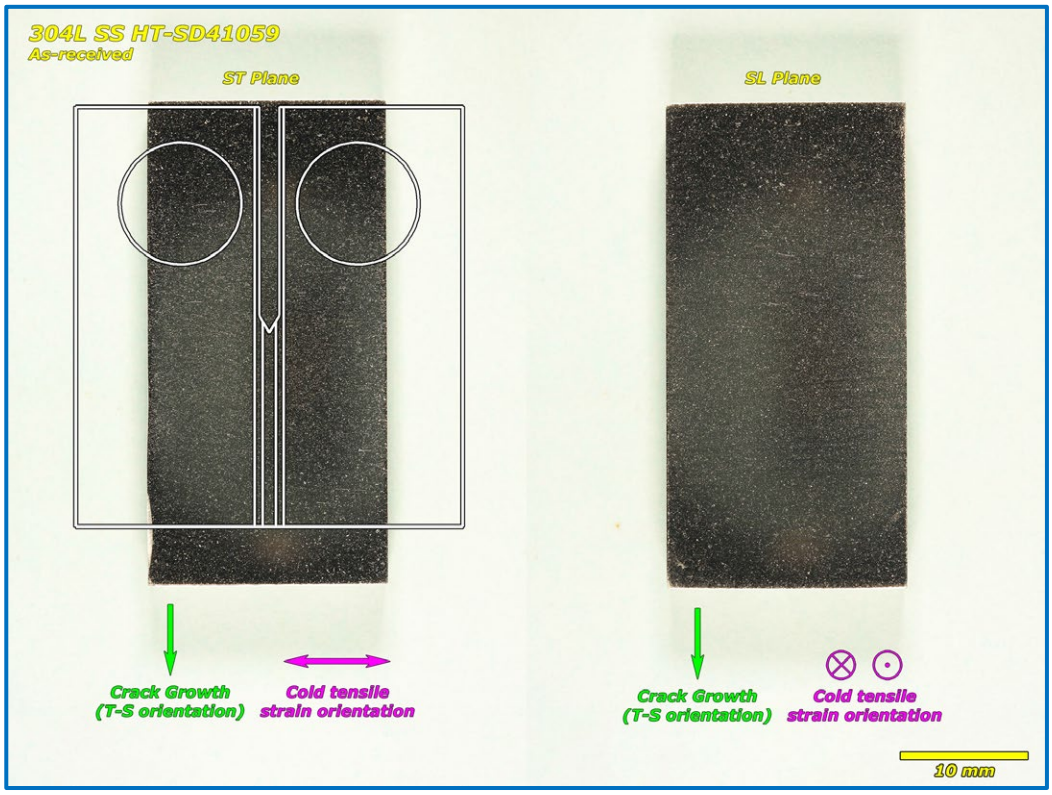

Figure 20. Low magnification bright field optical image of Heat P304L2 in the ST and SL plane showing microstructural variability from top to bottom of the plate.

6.3.3 Optically Observed Microstructure of Heat P316L1 (Heat D84W)

The microstructure presented in Figure 21 is typical of CCR materials. Grain banding is clearly present in the SL plane, but the grain shape is still equiaxed. The average grain size as taken from the CMTR is 38 µm. Twinning occurs with low-to-moderate frequency throughout the microstructure. Carbides and secondary phases appear infrequently throughout the overall microstructure, although they are sometimes observed to occur in high densities within individual grains. Figure 22 suggests a relatively uniform microstructure from top to bottom of the place except for in the very mid-thickness.

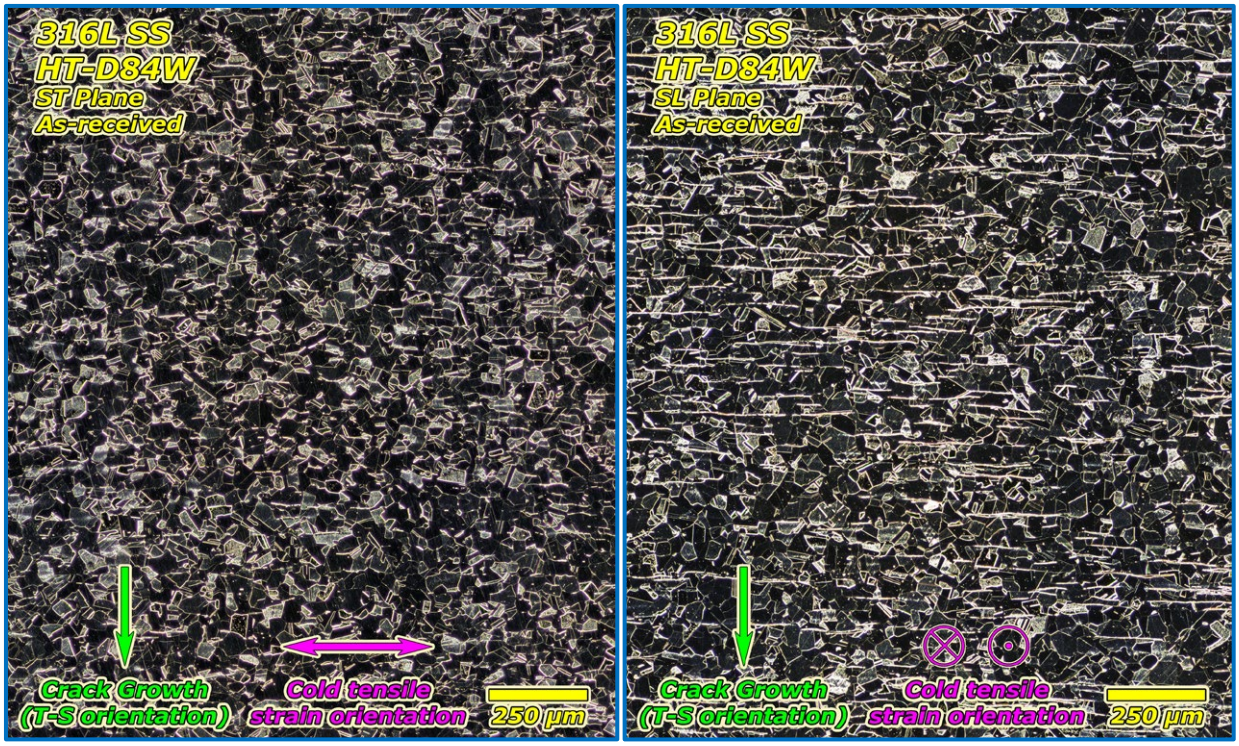

Figure 21. Dark field optical imaging of Heat P316L1 in the ST and SL plane relative to the plate shape and plate processing direction.

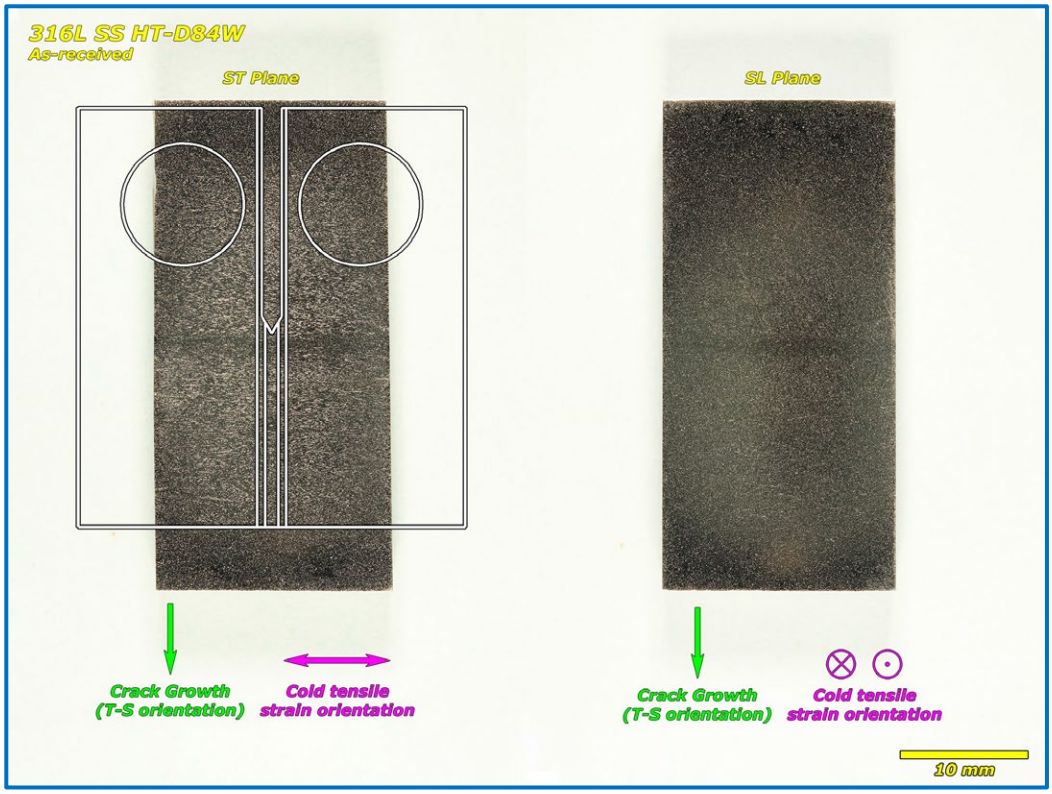

Figure 22. Low magnification bright field optical image of Heat P316L1 in the ST and SL plane showing microstructural variability from top to bottom of the plate.

6.4 Tensile Straining and Specimen Orientation

The tensile bar extraction and CISCC test specimen orientation plan is shown in Figure 23. As discussed earlier, a fraction of the CISCC tests will be conducted on materials that have been 10% cold worked by tensile straining. Further examples of SCC test specimen orientation relative to the tensile straining bars are provided in Figure 24. 26 0.5T CT specimens or 22 4PB specimens of tensile strained material can be machined from each 1 ft x 1 ft plate. With eight 12 inch x 12 inch plates of each material available, this allows for 104 CT specimens and 88 4PB specimens in total to be machined from each heat in a 10% tensile strained condition. Based on the SCC results that have been observed to-date (Section 7) where CISCC growth was readily observed in non-cold worked 304 and 304L, there is now a strong interest to CISCC test non-cold worked material. These specimens can readily be obtained from the remnants of the plates that were machined for tensile specimens.

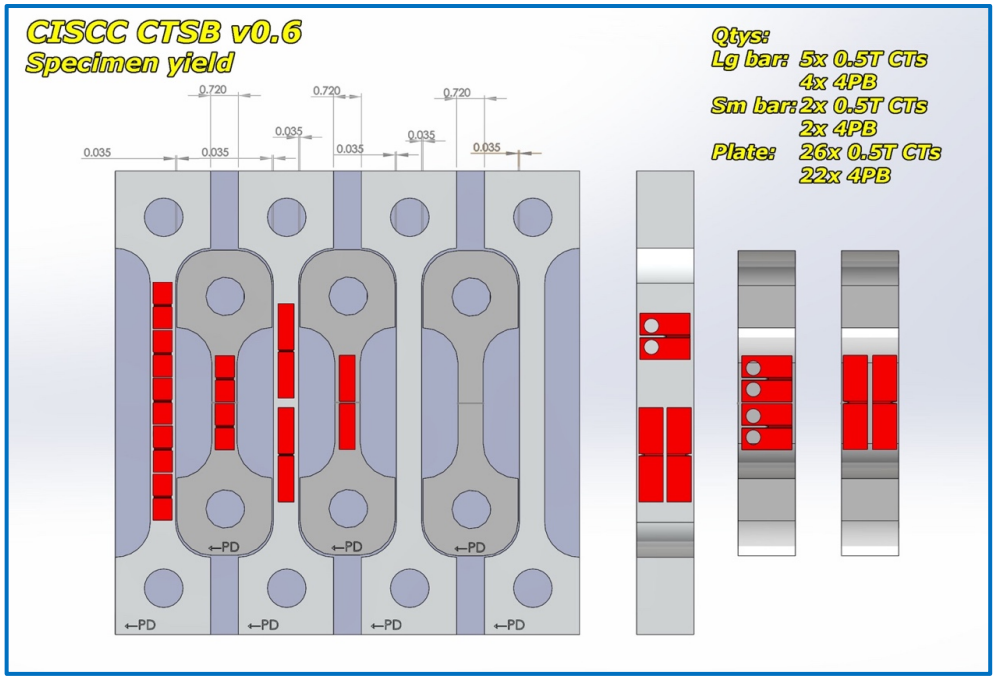

Figure 23. Orientation of tensile specimens and SCC test specimens relative to stainless steel plate dimensions and plate processing direction.

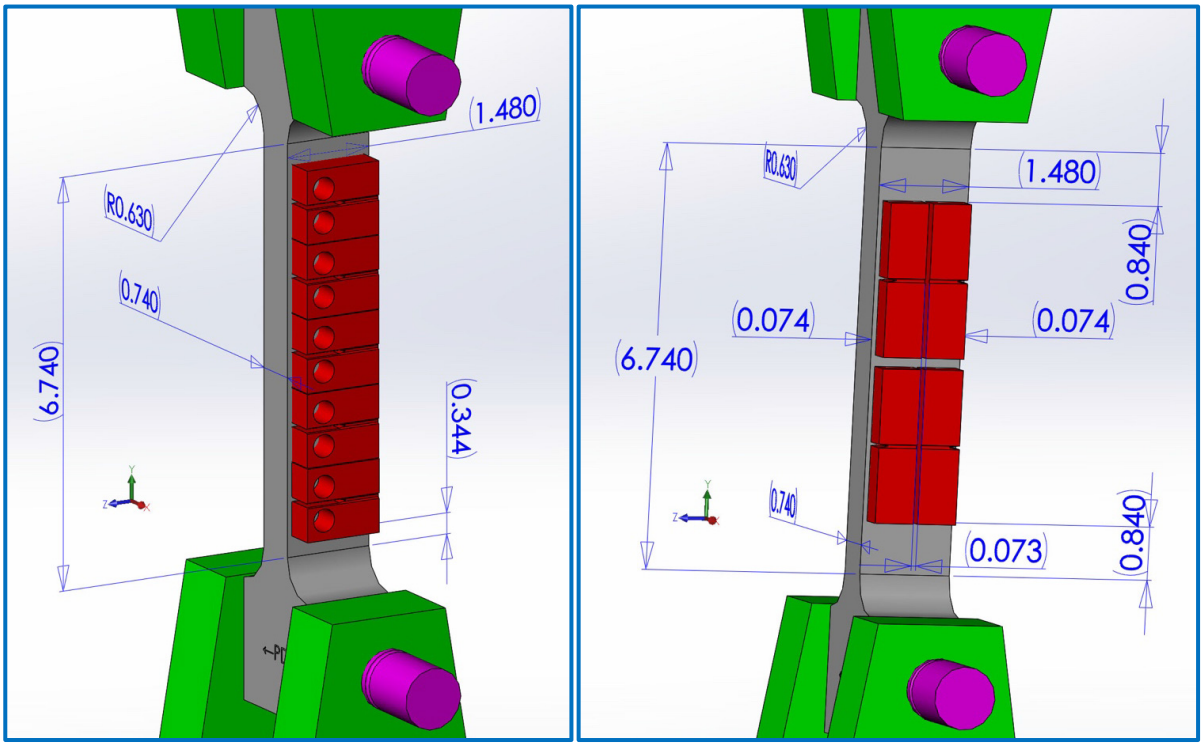

Figure 24. Orientation and quantity of 0.5T CT specimens and 4PB specimens that can be removed from a tensile specimen.

To aid in selecting a tensile specimen geometry that produces the most uniform strains in the gauge section, elastic-plastic finite element modelling (FEM) of the tensile straining was conducted using a representative constitutive equation for 304L SS assuming isotropic hardening. FEM of the originally selected tensile specimen design shown in Figure 24 revealed that this design did not provide a sufficient amount of material around the clevis pin to prevent significant straining of the specimen in that region. The clevis pin orientation had to be turned 90 degrees to eliminate this issue. Additional FE modelling of the tensile specimen taken to 10% plastic strain (Figure 25) revealed nearly uniform strain in the gauge section to within 10 mm of the start of the fillet, and then no more than 1% plastic strain variation covering the remaining 10 mm distance to the fillet. In the region of where a CISCC test specimen would be cut near the fillet, the variation is no more than ± 0.5% plastic strain.

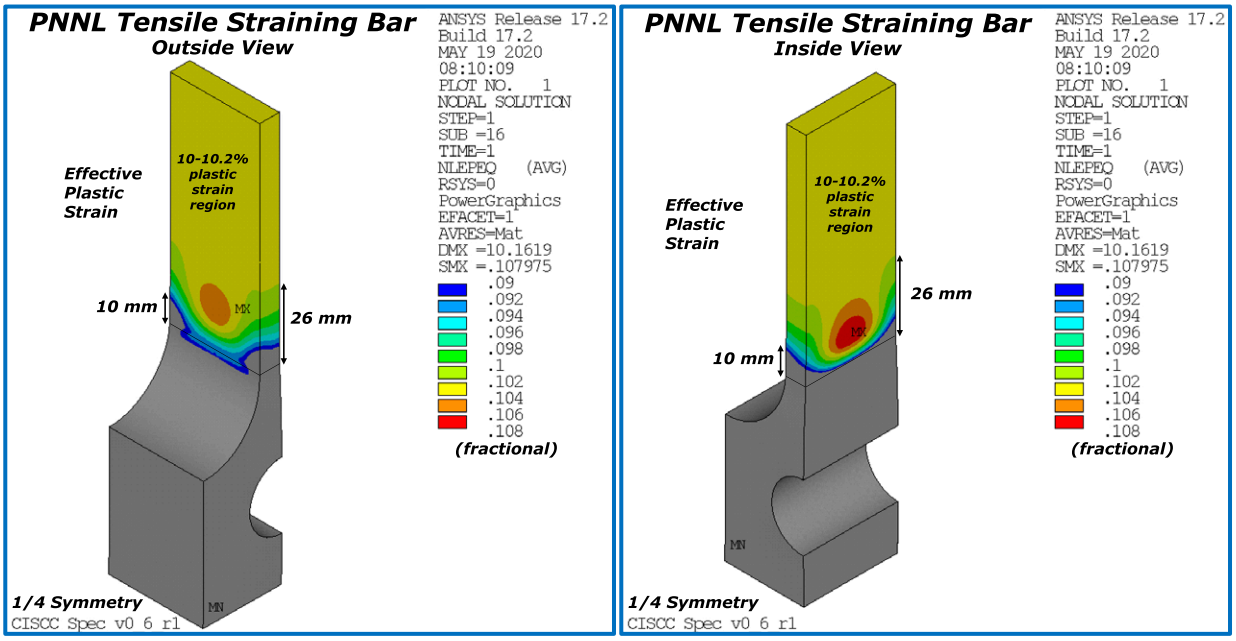

Figure 25. Finite element-based estimate of the plastic strain in the gauge region of tensile bars that will be used to extract CISCC test specimens.

Straining of four tensile bars of each task material has been completed. Straining was performed in a 120 kip load frame at a crosshead speed of 0.125 inch/min which corresponds to a strain rate of approximately 3.5×10^{-4}/sec. Strain was monitored with an extensometer attached to the center of the gauge section, covering a length along the gauge section of approximately 2 inches. The resolution of the extensometer is 0.002% strain. Stress versus strain data from all specimens were obtained with the tensile straining response of the first tensile specimen from heat P304L1 provided as an example in Figure 26. The stress versus strain response is typical for 300 series stainless steel but note that the observed yield stress is 20 MPa below the reported value in the CMTR. To simplify the straining process and make it easier to obtain the same strain from specimen to specimen, total strain rather than plastic strain was monitored and stopped at 10% strain. This results in a plastic strain value that is in the range of 9.6-9.9%.

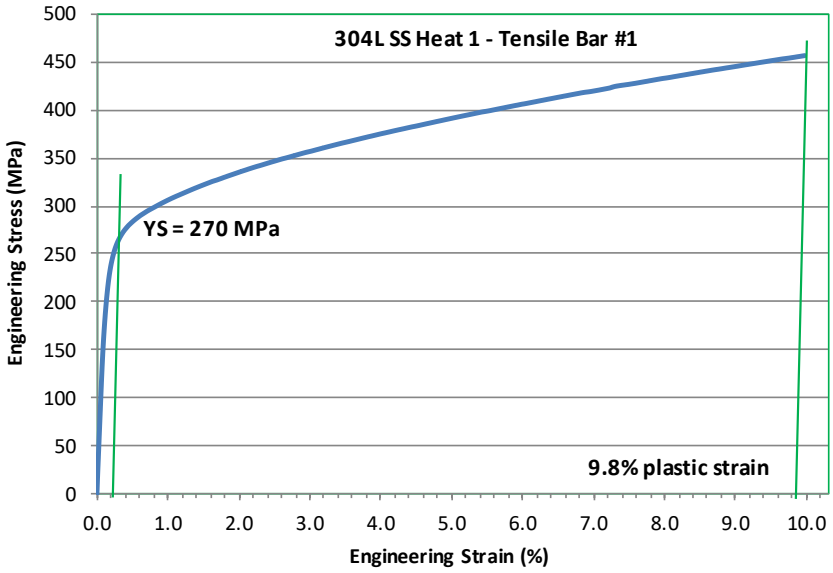

Figure 26. Tensile straining response of the first specimen of 304L SS Heat 1.

This page is intentionally left blank.

7. CISCC TESTING RESULTS

7.1 Overview

As discussed earlier in the report CISCC growth rate testing is being conducted in brine solutions for the first 1-2 years to provide a basis for comparison with the CISCC response in deliquescent humid air conditions. For FY20, tests on two specimens have been completed while testing on another four specimens is in-progress. Work limitations due to COVID-19 prevented more tests from being conducted. However, the six specimens presented here generally exhibit self-consistent response that falls within the trend band from the literature **[20]**.

7.2 Air Fatigue CGR Measurements

Air fatigue crack growth rate (AFCGR) data provide a valuable point of reference for understanding corrosion fatigue response during crack transitioning steps utilizing cyclic loading. At higher cyclic loading frequencies, e.g., higher than 0.1 Hz for these materials in NaCl-saturated water, when there is insufficient time for stress corrosion or general corrosion to take place, the CGR will match the AFCGR at the same temperature with the same cyclic loading conditions. As the cyclic loading frequency decreased, corrosion or stress corrosion can begin to play a role in the crack growth response. If the environment favors stress corrosion, then the corrosion fatigue CGR will be higher than the AFCGR. However, if general or localized corrosion is high, then the environmental response can drop below the AFCGR value due to crack tip blunting reducing the stress intensity **[21, 22]**. Thus, during a CISCC test, knowing the AFCGR response of a material is a powerful guide for test management. To this end, a limited amount of AFCGR data have been obtained on one heat of 304L. In particular, data were obtained in 40°C air at stress intensity factors of 20 and 25 MPa√m at the cyclic loading conditions that PNNL has traditionally used for SCCGR testing as shown in Figure 27. The data fit to both cyclic loading frequency and stress intensity to give the empirical relation shown in the figure. Interestingly, the fit to cyclic loading frequency had a stress exponent slightly less than one. This may be due to a very slight effect of the air environment on crack growth response.

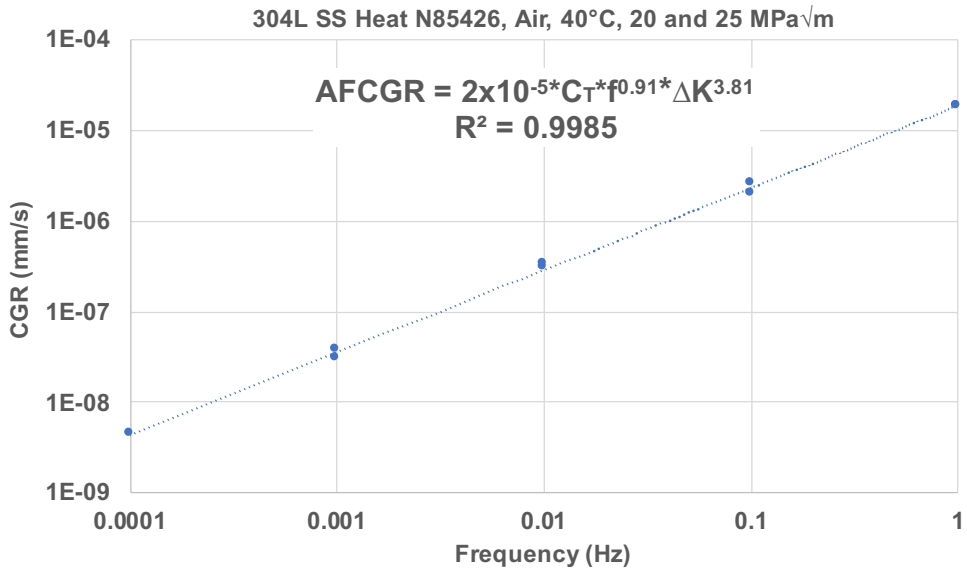

Figure 27. AFCGR response of 304L SS at 40°C for stress intensities of 20 and 25 MPa√m.

7.3 CISCC Tests

7.3.1 CT187 & CT188 – 304L SS Heat N85426, As-Received, Specimens 1 & 2

This is the first CISCC test conducted on the CISCC testing task at PNNL, and it took place before and during test system optimization activities. This test was conducted at 40°C with non-filtered water that was simultaneously aerated and agitated using an air bubbler within the environmental chamber. Several different bubbler configurations were evaluated during this test. The specimens are cut from a non-task heat (i.e., cut from a heat of material other than those described in Section 6) of 304L that was readily available for use.

An overview of the test is provided in Figure 28. The first 150 hours of the test was dedicated to observing DCPD noise levels. Testing subsequently began at 27 MPa√m following crack transitioning steps typically used by PNNL for LWR SCC growth tests. This stress intensity was selected to be near or above the threshold stress intensity for CISCC growth based on the results of Speidel, Shaikh, and Kosaki **[23-25]**. Speidel reported a threshold stress intensity of ~27 MPa√m, Shaikh reported <20 MPa√m, and Kosaki reported crack growth occurred at the stress intensity as low as ~1 MPa√m.

During transitioning at moderate to gentle continuous cyclic loading conditions, the crack growth response of both specimens was nearly identical to each other as can be seen in Figure 29. However, when a 2.5 hr hold at K_{max} was added to the cyclic loading as shown Figure 30 between 250 and 800 hours, the response of the specimens bifurcated with CT187 maintaining steady growth and CT188 trending to a no-growth condition. Air fatigue testing had not yet been conducted to provide a point of comparison for the corrosion fatigue data obtained during transitioning, but each change in cyclic loading condition performed in this test reduced the effective cyclic loading frequency by a factor of 10, and for air fatigue testing, the CGR would also drop by a factor of ~10x. This can be a useful point of reference because materials exhibiting SCC response generally will show a less than 10x decrease in CGR The decrease in CGR for CT187&88 from 0.01 Hz cyclic loading to 980s/20s cyclic loading (0.001 Hz effective frequency) was 17x, while the decrease in CGR from 980s/20s cyclic loading to 980s/20s cyclic loading with a 2.5 hr hold (0.0001 Hz effective frequency) was only 1.22x for CT187. Thus, the CGR of the specimens after the first change in loading frequency decreased more than would occur during an air fatigue test suggesting a loss of cracking susceptibility, while for the second change in loading condition for CT187 indicated a strong corrosion fatigue response.

Because this was our first CISCC test, and CT187 was showing steady growth at the cycle+hold loading condition, the decision was made to change to constant load conditions to obtain a CISCC growth rate measurement. As can be seen in Figure 30, CT187 maintained a steady growth response with a final CISCCGR of ~1.7×10^{-7} mm/s at 27 MPa√m. This is at the high end of the trend band at 40°C found in a literature review of CISCC growth rate data by Bryan **[20]**. The no-growth response of CT188 during cycle+hold and constant load can have two possible explanations. The first is that something happened to the crack to inhibit crack growth. Considering that NaCl can produce a strong localized corrosion response in 304 SS, a likely reason that cracking is inhibited is crack tip blunting. When the crack tip blunts, the stress intensity at the crack tip drops dramatically, and crack growth stops completely. Another possible explanation is that the DCPD-based in-situ crack length measurement method was not tracking crack length accurately. In particular, if a significant number of electrically conducting bridges form behind the crack front such as a conducting corrosion product, then DCPD will not accurately track the crack extension. The test was subsequently stopped to perform test system modifications. A post-test examination of the specimens has not yet been performed due to COVID-19 work restrictions, so the response of either specimen has not yet been confirmed by crack surface observations. This will take place in early FY21.

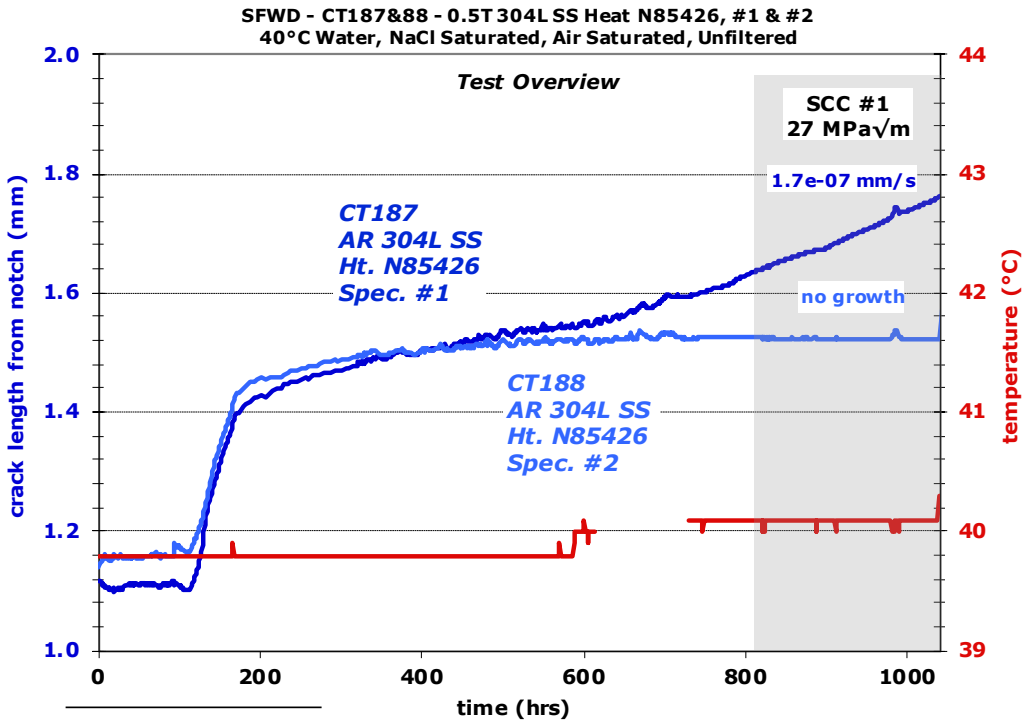

Figure 28. Overview of crack growth response of two 304L SS heat N85426 specimens in an as-received condition.

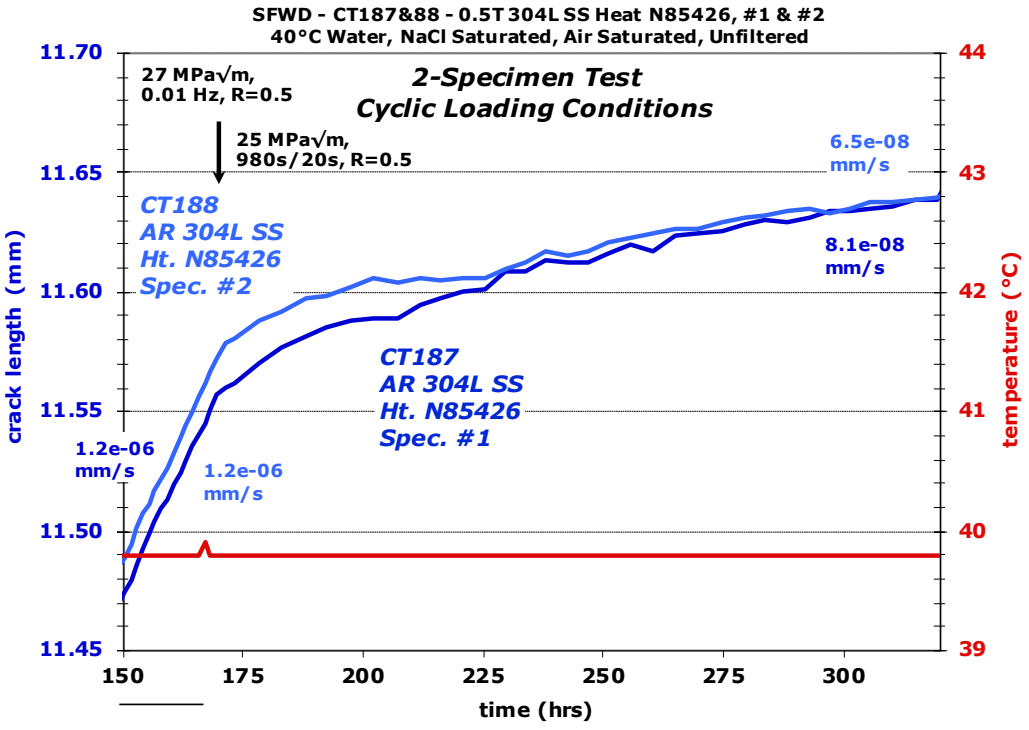

Figure 29. Cyclic loading crack growth response at 27 MPa√m of two 304L SS heat N85426 specimens in an as-received condition.

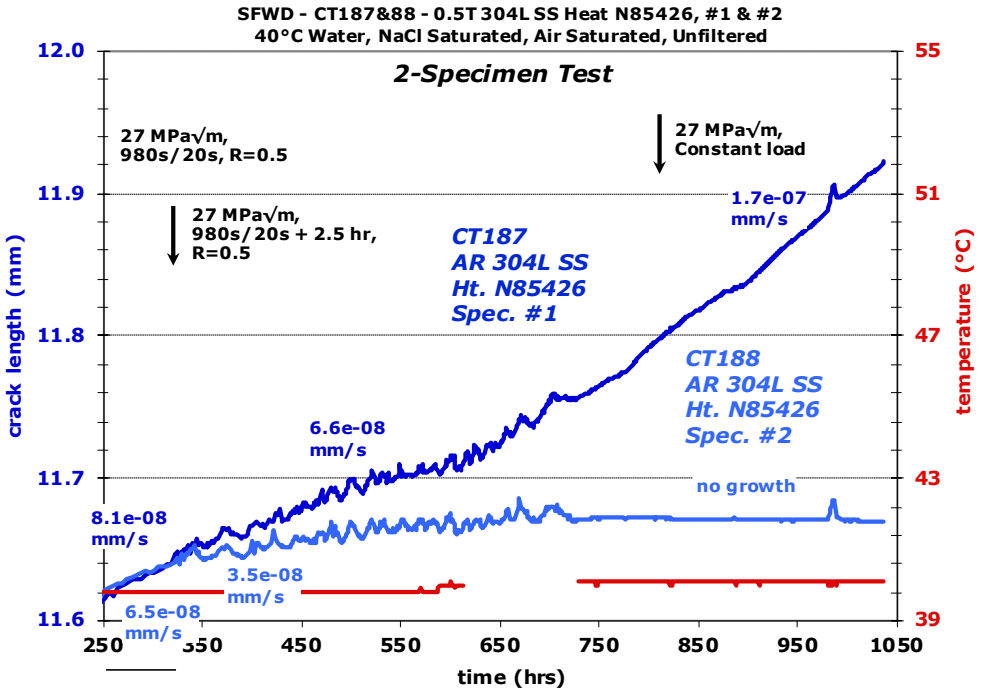

Figure 30. Cyclic loading and constant load SCC crack growth response at 27 MPa√m of two 304L SS heat N85426 specimens in an as-received condition.

7.3.2 CT189 & CT190 – 304L SS Heat N85426, As-Received, Specimens 3 & 4

These are the third and fourth specimens of heat N85426 to be tested in a brine solution. These two specimens were previously used to measure air fatigue response needed to establish the degree of corrosion fatigue behavior during transitioning steps under environmental testing conditions. This material is not one of the planned task heats - those are still be prepared for SCC testing. This test is being conducted at 40°C with a salt content that is 97% of the fully saturated content. Salt content is being kept slightly below the saturation level because during early testing, it was found that air saturating the water could cause a small amount of salt to precipitate out of solution, and the salt would subsequently clog the water pump. The water is air saturated and passes through a 1 µm filter.

For this test, the water nozzles in the environmental chamber are oriented to provide a gentle flow of water into the crack notch. This is being done to limit the degree of attached air bubble formation in the specimen notch. In general, we are observing that air bubbles nucleate, grow, and remain present on many of the surfaces in the environmental chamber, including in the crack notch. There is some concern that these bubbles may be present on the root of the notch and potentially affect the exposure of the crack to the bulk water environment. While we have yet to document that this is actually occurring, we have found that directing water into the notch of the specimens is preventing any bubbles from forming in the mouth. This behavior will be further assessed in the coming months.

An overview of the DCPD-based crack growth response to date is shown in Figure 31. During transitioning steps prior to the constant load observation at 26 MPa√m, steady crack growth was observed at 0.1 Hz, 0.01 Hz, and 980s/20s load cycling (Figure 32), each covering at least 100 µm of crack extension (thus traversing multiple grains which provides confidence in the observed crack growth rate), while at cycle+hold conditions, the CGR dropped over a period of ~200 hours and then remained relatively steady. During the 26 MPa√m constant load SCC observation (Figure 33), both specimens exhibited fairly steady response that was essentially unchanged from the preceding cycle+hold step.

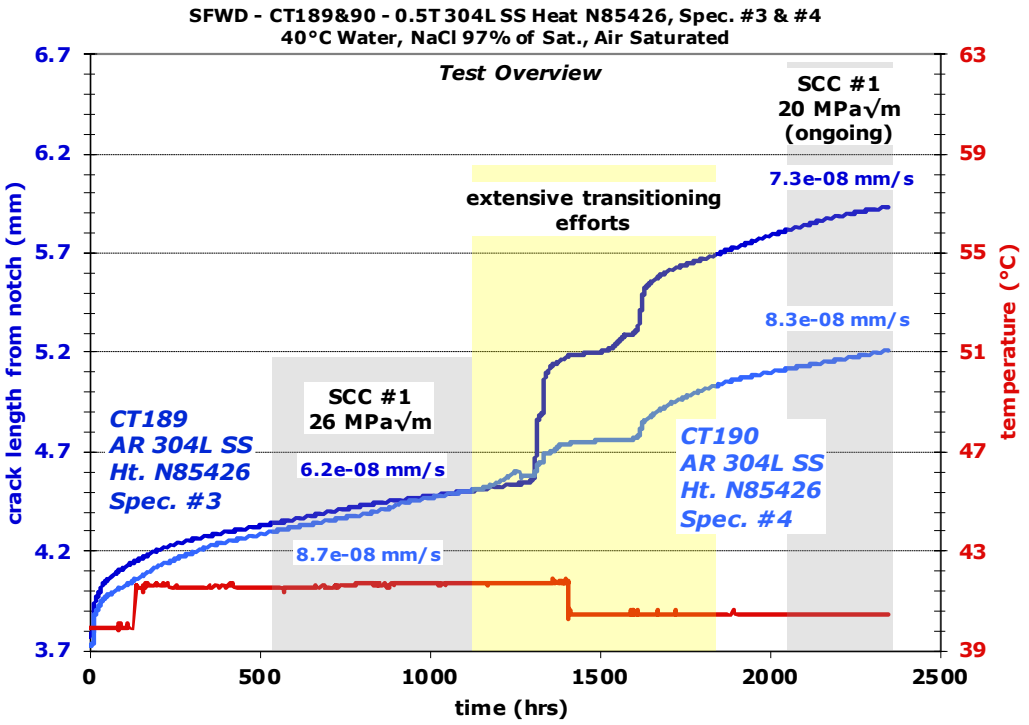

Figure 31. Overview of crack growth response of two 304L SS heat N85426 specimens in an as-received condition.

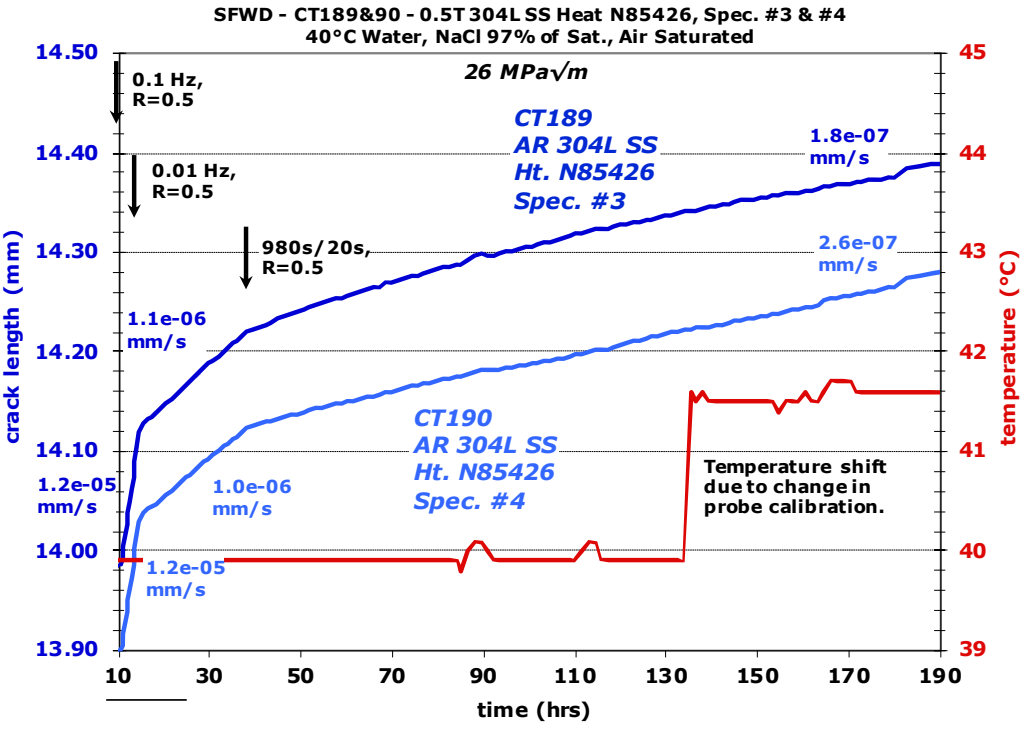

Figure 32. Crack growth response of two 304L SS heat N85426 specimens during initial transitioning steps.

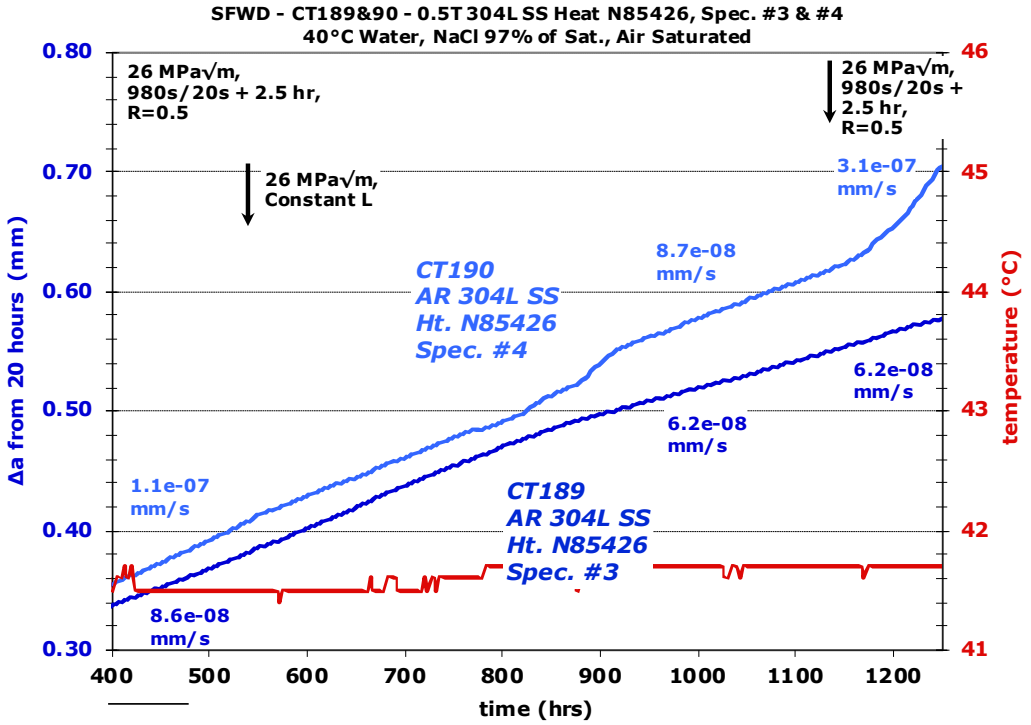

Figure 33. Constant load SCC crack growth response at 26 MPa√m of two 304L SS heat N85426 specimens in an as-received condition.

The cycle+hold response after the constant load observation (also Figure 33) was similar to the response before constant load, so the decision was made to drop to 20 MPa√m via a stepped reduction in stress intensity as a linear function of crack length with the response shown in Figure 34. This approach to reducing stress intensity is referred to as dK/da. The dK/da process for the change from 26 to 20 MPa√m initially began at 0.01 Hz with R = 0.5, but extremely muted CGR response was observed, so frequency was increased to 0.1 Hz again with muted response. It wasn't until setting the cyclic loading frequency to 1 Hz did the specimens show more consistent response, however CT190 still exhibited somewhat muted response.

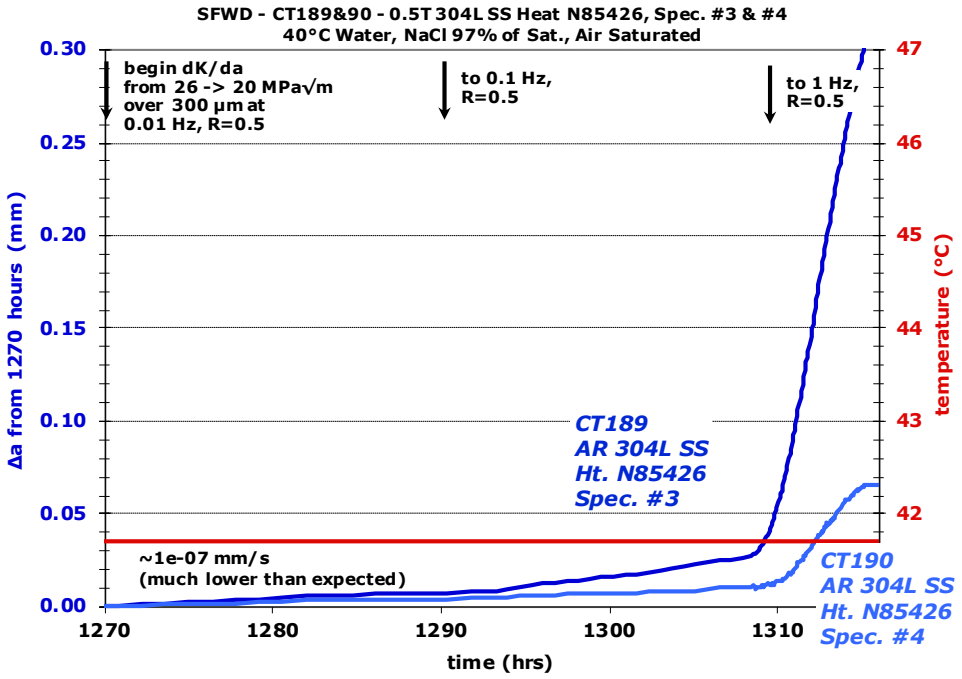

Figure 34. dK/da from 26 down to 20 MPa√m for CT189&90.

After arriving at a 20 MPa√m, both specimens again showed muted response (below AFCGR values) during initial transitioning steps towards constant load, so once again, progressively more aggressive cyclic loading conditions (higher frequency and/or lower R values) were applied until corrosion fatigue CGRs began to increase towards air CGR values at the same cyclic loading conditions. These steps are summarized in Figure 35 as indicated by the "More aggressive load cycling" label. Transitioning then moved towards more gentle cyclic loading conditions where very high corrosion fatigue CGRs were observed as shown by the "More gentle load cycling" portion of the environment versus air plot at 20 MPa√m. The crack growth response during these progressively more gentle steps is shown in Figure 36. The initial muted crack growth response followed by a strong corrosion fatigue response suggests that at some point, either during or after the 26 MPa√m SCC observation, the crack had become more resistant to general SCC behavior. The fact that the cyclic loading CGRs in brine fell below AFCGR values suggest that the crack tip had become blunted (and thus strongly reduced the actual crack tip stress intensity). If the crack had blunted during the 26 MPa√m constant load observation, this calls into question what was actually being measured during that SCC observation. It may be possible that substantial crack tip corrosion was occurring and giving the indicated rapid crack advance at 26 MPa√m. Post-test observations of the specimens should clarify this.

This test was recently set to constant load for a CISCCGR observation, also shown in Figure 36. The propagation rate of CT189 has decreased slightly from the cycle+hold value while CT190 is exhibiting a steady propagation rate that is almost the same as the cycle+hold value. The growth rates are in the same range as those observed for CISCC growth at 27 MPa√m. This observation will continue until at least 100 µm of crack extension has been attained to help provide confidence in the observed values. After completion of this step, testing will continue at progressively lower K values until a no growth condition is reached during a CISCC observation.

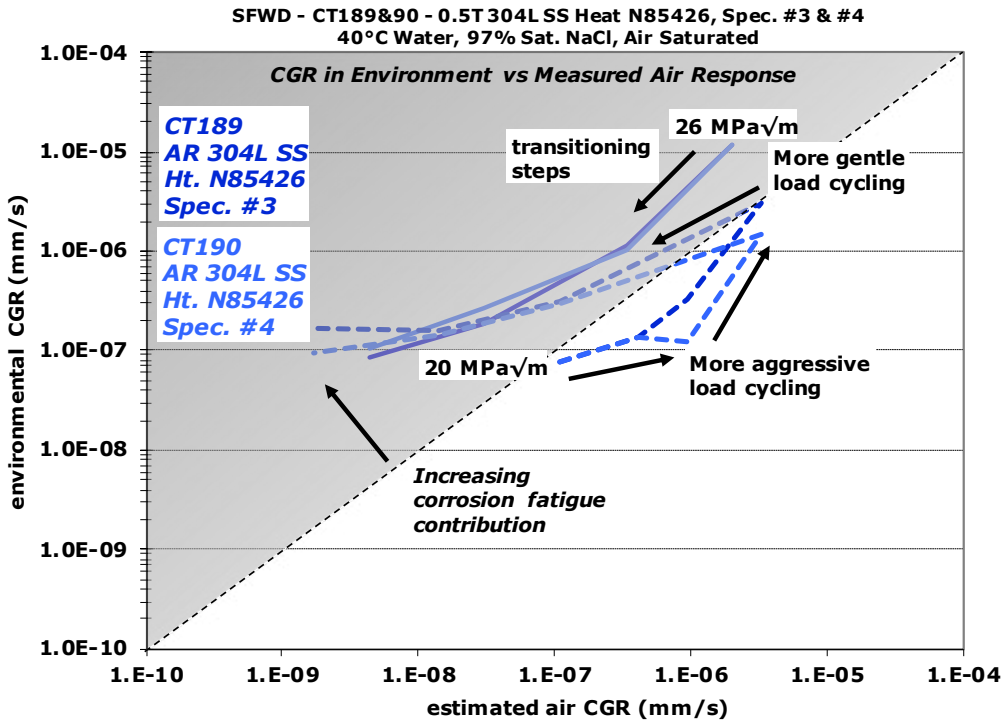

Figure 35. Environment versus estimated air response of two 304L SS heat N84526 specimens in an as-received condition.

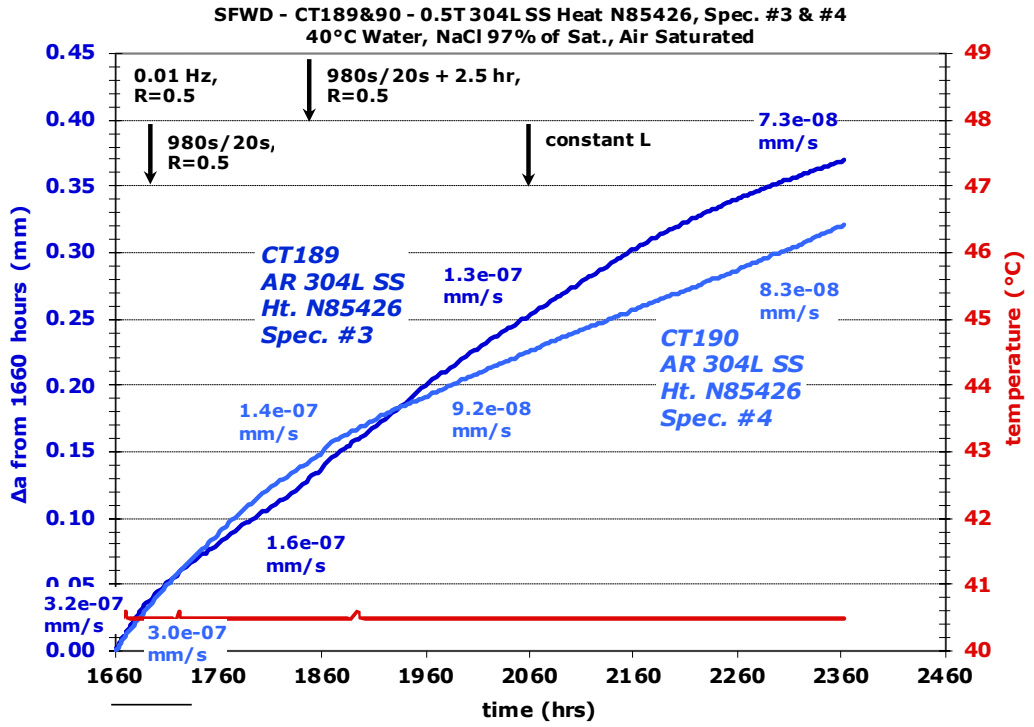

Figure 36. Crack transitioning and constant load behavior at 20 MPa√m for CT189&90.

7.3.3 CT199 & CT200 – 304 SS Heat 710183-1B, Sensitized

This is an ongoing test on two sensitized 304 SS (non-L grade) specimens. These specimens are leftovers from an LWR SCC testing program at PNNL about 14 years ago. During previous CISCC testing of other specimens using a fully saturated NaCl solution, salt precipitation was observed during strong aeration, so for this test, a salt content of 97% of the saturation limit of water was selected to prevent salt precipitation. Air saturation of the brine solution is achieved using the jet aeration method previously described. Another feature that has been implemented in the test systems is water filtration - a high volume 1 um filter is being used to remove large corrosion products from the water. Test temperature is 40°C.

An overview to-date of the DCPD-based crack growth response shown in Figure 37. Testing at 25 MPa√m in water saturated with NaCl at 40°C has already been completed with measured constant load SCCGRs of 3.4×10^{-8} mm/s (1.1 mm/yr) and 6.8×10^{-8} mm/s (2.1 mm/yr) for CT199 and CT200, respectively as shown in Figure 38. The first 500 hours of CISCCGR response at 21 MPa√m is shown in Figure 39. CT199 is exhibiting very steady response while CT200 had a slight downward shift in CGR at about 250 hours of exposure at constant load. These CISCCGRs are nearly as high as the values observed at 26 MPa√m. Constant load will be maintained for at least 500 hours, and after which, stress intensity will be transitioned down to 17 MPa√m. Response at continually lower stress intensities will be performed until a no-growth condition is attained.

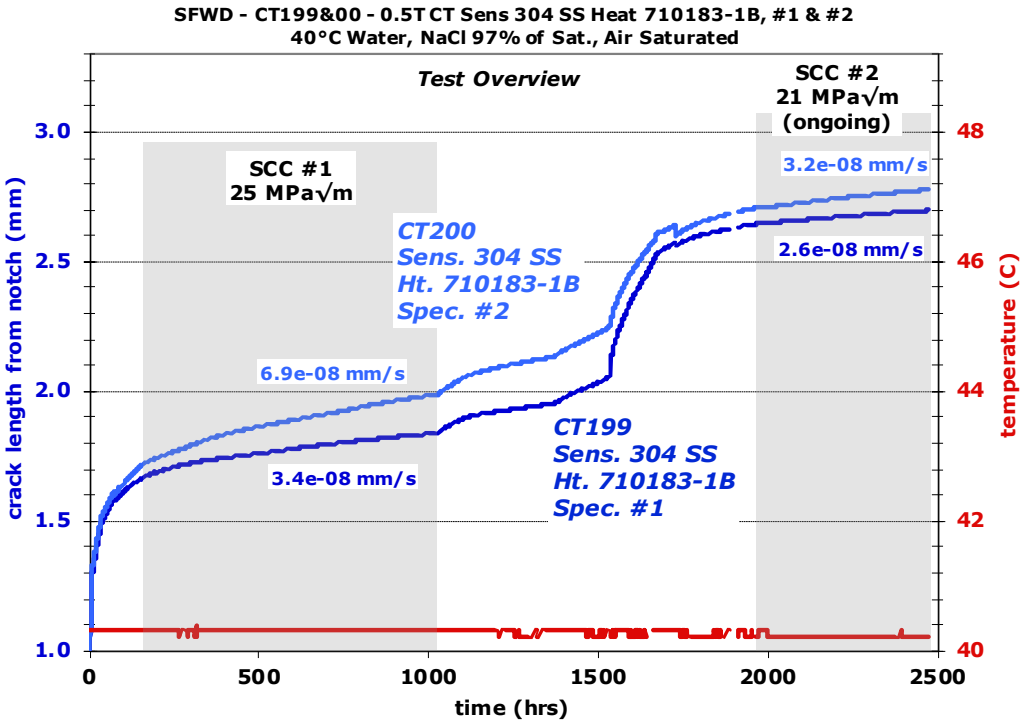

Figure 37. Overview plot of a crack growth test on two 304 SS heat 710183-1B specimens in a sensitized condition.

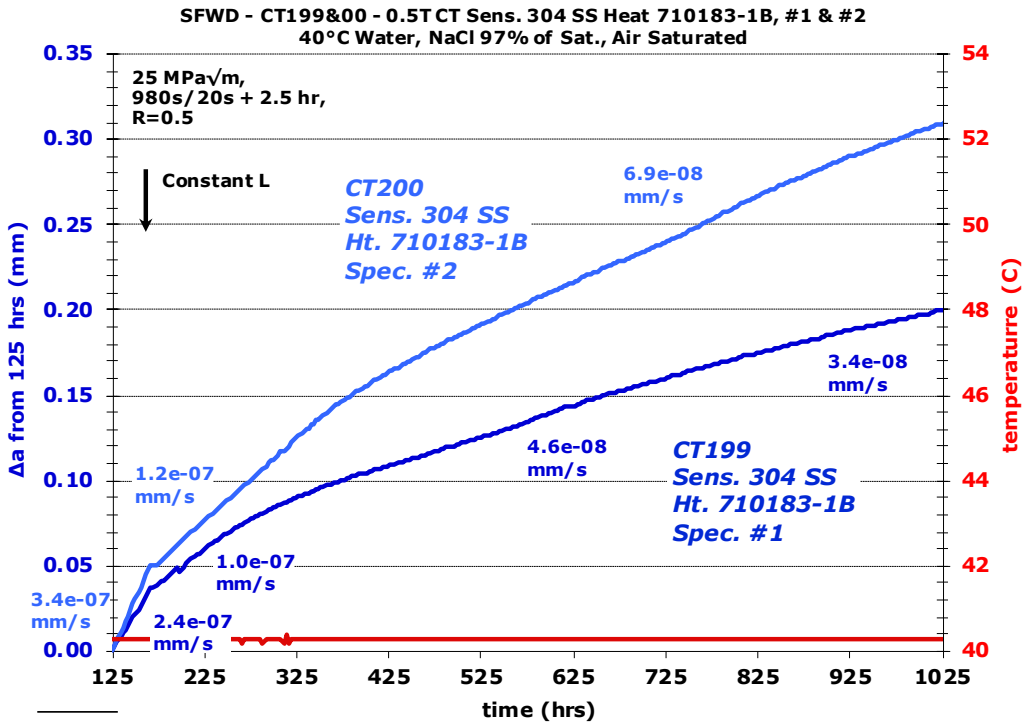

Figure 38. Stress corrosion crack growth response during constant load at 25 MPa√m of two 304 SS heat 710183-1B specimens in a sensitized condition.

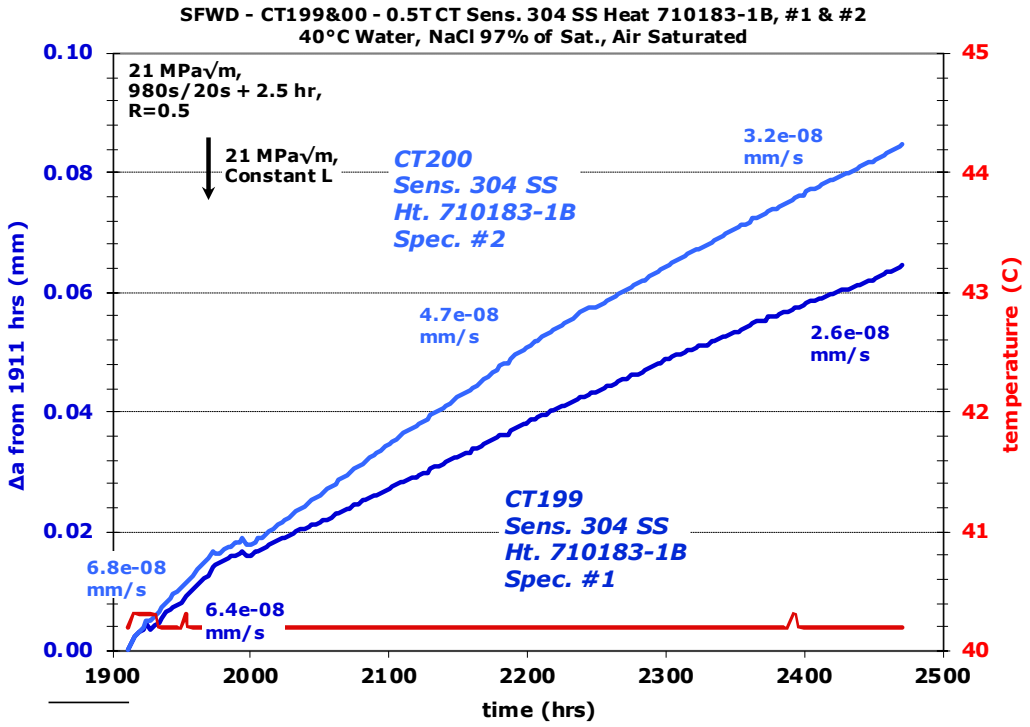

Figure 39. Stress corrosion crack growth response during the first ~500 hours at constant load at 21 MPa√m for two 304 SS heat 710183-1B specimens in a sensitized condition.

During this test, techniques for reducing stress intensity while maintaining representative CISCC response were evaluated. A reduction in stress intensity typically requires extending the crack length either during or after the stress intensity reduction to grow the crack out of the plastic zone created by the crack at higher stress intensity. This crack extension is needed because the microstructure and strength of the plastic zone at different stress intensities can affect the crack growth response. Low strength materials such as mill annealed stainless steel used to make the storage containers will have a relatively large plastic zone for a given stress intensity. At 25 MPa√m, the plastic zone is of the order of 0.3-2 mm in size depending on the approach used to determine the value, i.e., the plane strain or plane stress approach. Even the low side of this range is fairly large and would take a substantial amount of time to grow the crack this distance and then subsequently transition back to SCC conditions. Growing the crack these large distances also uses up substantial amounts of the specimens.

As a means to assess the need to extend the crack by distances approximately equal to the size of the plastic zone, the stress intensity reduction process was performed over an amount of crack extension equal to a small fraction of the estimated plastic zone size, and then the reduction was repeated, this time over an amount of crack extension equal to a large fraction of the estimated plastic zone size. After the stress intensity reductions, cyclic loading CGR response was measured and compared. The first stress intensity reduction, from 25 to 21 MPa√m, was performed over a crack extension of 30-40 µm (depending on the specimen) as shown in Figure 40. After returning to 25 MPa√m, stress intensity was again reduced, this time while covering 300-400 µm of crack extension, and this was followed by another 200-250 µm of crack extension as shown in Figure 41 and Figure 42. Cyclic loading response at 980s/20s+2.5 hr with R=0.5 after the two different stress intensity reductions was virtually identical. For the 30-40 µm extension, it was 5-7x10^{-8} mm/s (Figure 40) while for the 500-600 µm crack extension, the cycle+hold CGR was 6.5-7x10^{-8} mm/s (Figure 42). These ranges of CGR values are almost completely overlap. Another comparison can also be made using the environment versus air response plot in Figure 43 where the response is compared at several different cyclic loading conditions and also compared to the response at 25 MPa√m. The cyclic loading response for the two different amounts of crack extensions during and after stress intensity reduction overlap, indicating that for modest reductions in stress intensity in these materials, extending the crack by the size of the plastic zone does not appear to be necessary. Knowing this will allow assessment of crack growth versus stress intensity to be accomplished within a shorter period.

Environment versus air response at 25 and 21 MPa√m can be compared in Figure 43. The slope of the trend during gentle cyclic loading conditions is virtually identical for the two different stress intensities. It will be interesting to see whether the parallel response remains at lower stress intensity. Another important aspect to mention is that strong corrosion fatigue response was observed at 21 MPa√m. This is a reasonable indicator that stress corrosion crack growth will occur at constant load conditions.

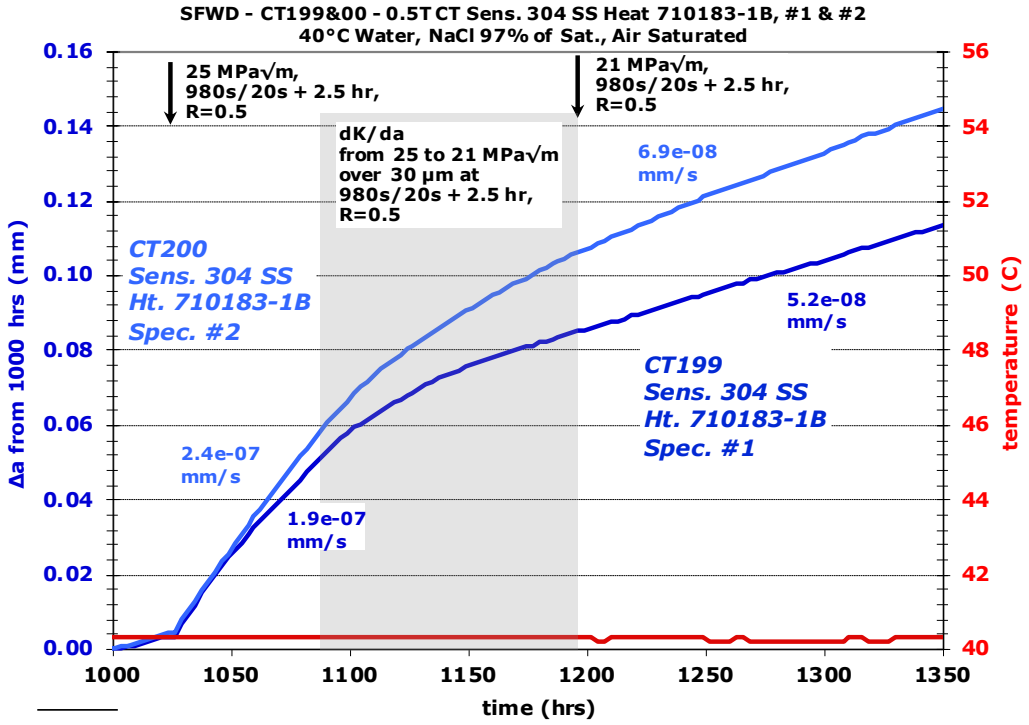

Figure 40. Stress intensity reduction from 25 to 21 MPa√m over 30-40 µm and subsequent cycle+hold loading response for two sensitized 304 SS heat 710183-1B specimens.

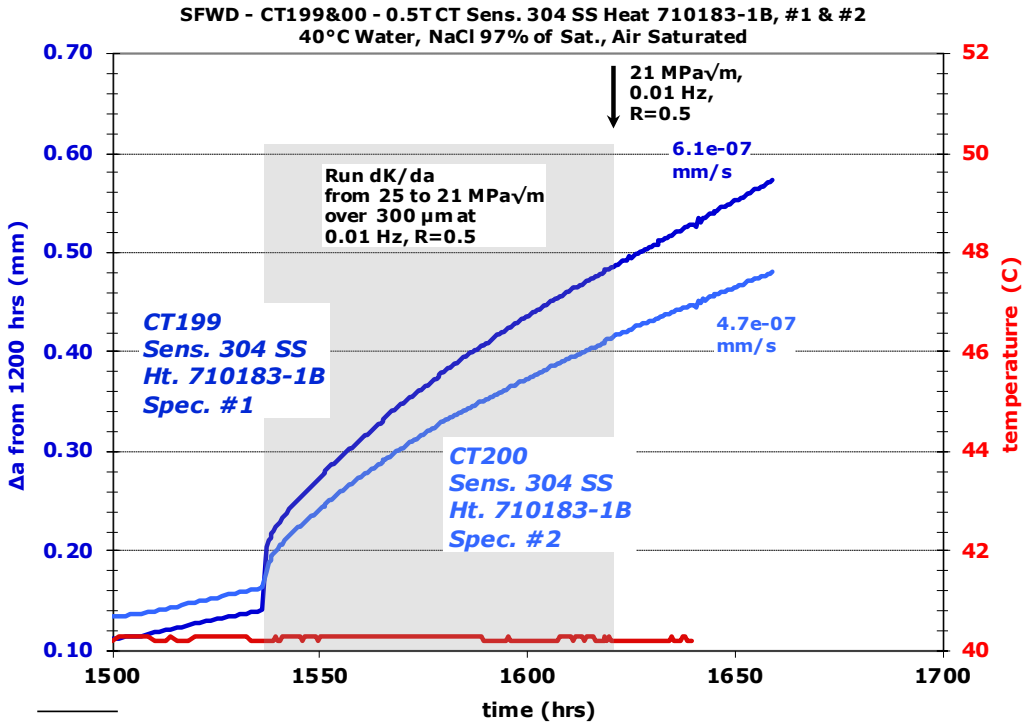

Figure 41. Stress intensity reduction from 25 to 21 MPa√m over 200-300 µm and subsequent observation under 0.01 Hz cyclic loading for two sensitized 304 SS heat 710183-1B specimens.

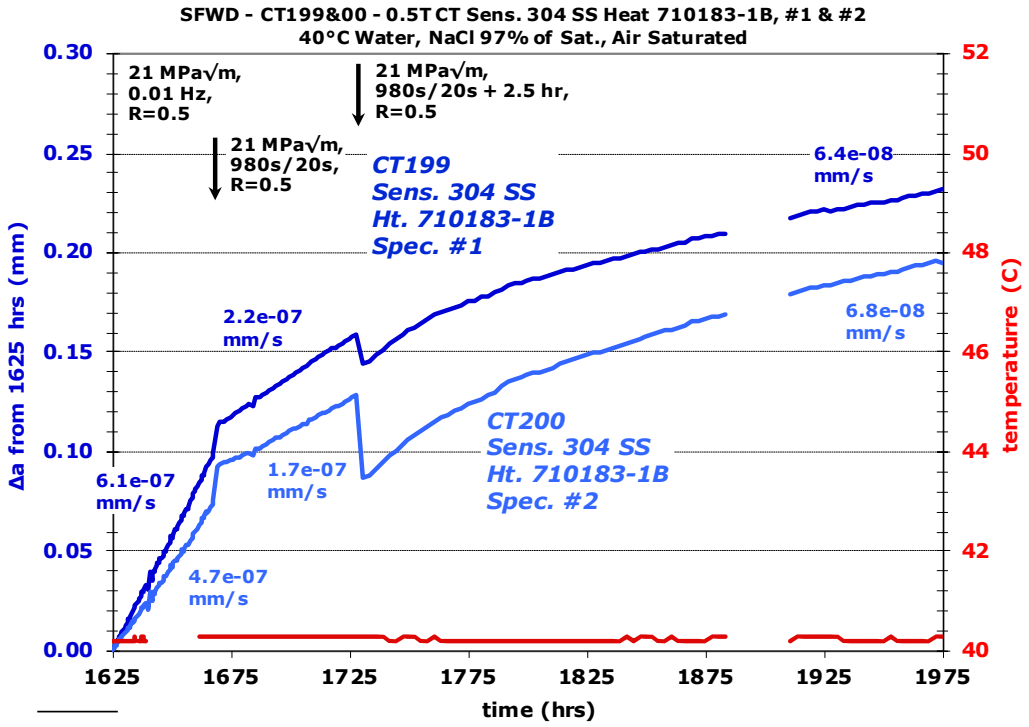

Figure 42. Crack growth response during transitioning steps at 21 MPa√m for two 304 SS heat 710183-1B specimens in a sensitized condition.

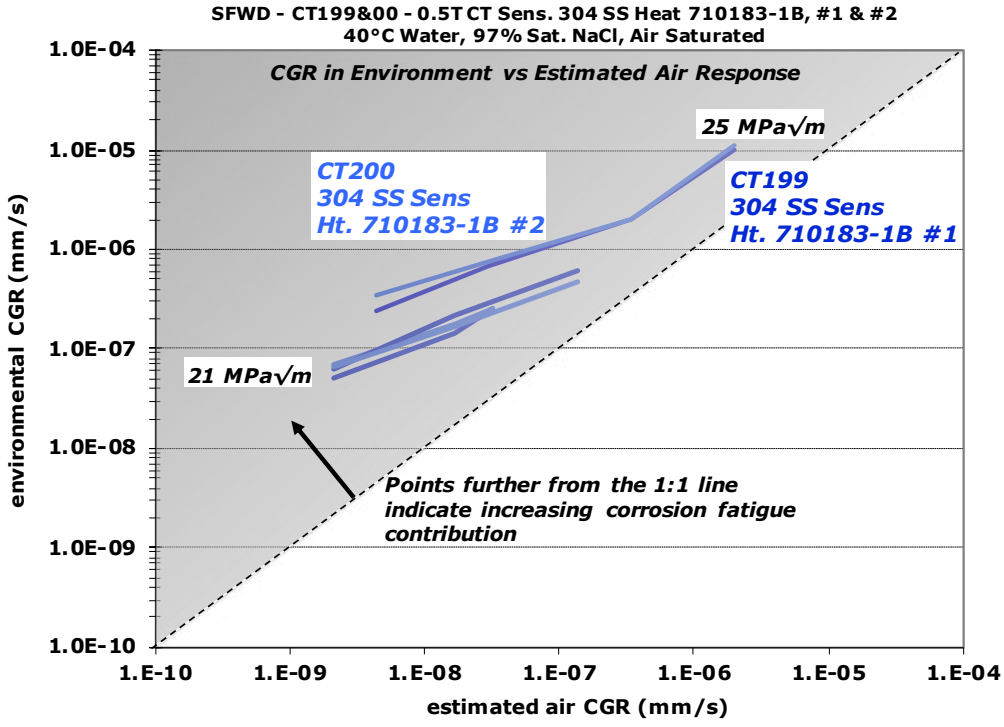

Figure 43. Environment versus estimated air response of two 304 SS heat 710183-1B specimens in a sensitized condition.

7.4 Discussion of Test Data

The seven CISCC growth rate data points that have been obtained thus far at PNNL in immersed conditions are ranging from $2.6x10^{-8}$ mm/s to $1.7x10^{-7}$ mm/s and match up well with a literature compilation of atmospheric and immersed CISCC growth rate data assembled by Bryan **[20],** as shown in Figure 44. This provides a degree of confidence that the PNNL testing methodologies are providing data that are consistent with prior studies.

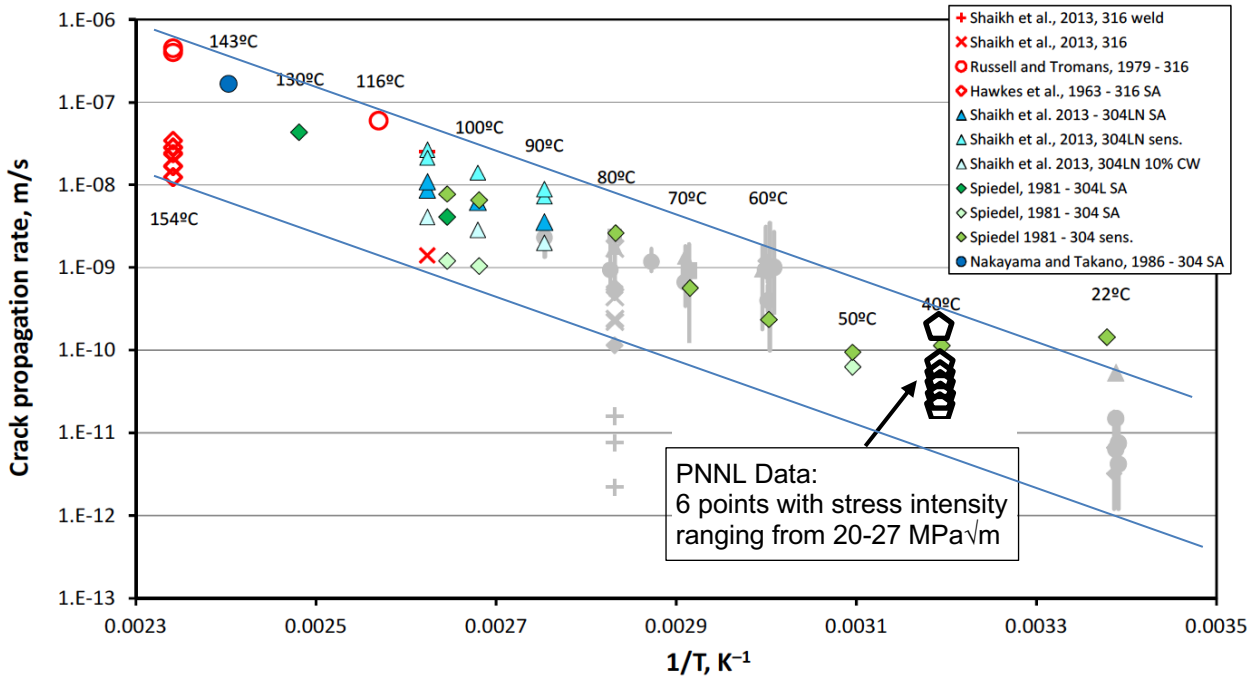

Figure 44. Current PNNL CISCCGR data added to SNL literature compilation [20]. SNL compilation in gray are from atmospheric evaluations while immersed are colored.

It is generally thought that stainless steels in concentrated salt water conditions will exhibit no SCC until reaching a threshold K level, after which the CISCCGR will be independent of stress intensity. One possibility for why a threshold behavior has been observed is that previous researchers may have had challenges measuring low crack growth rates and/or performing effective transitioning. Those results have been obtained using post-test evaluation of crack length on passively loaded specimens where no active test management is performed **[23-25]**. Considering the difficulty in obtaining corrosion fatigue and stress corrosion response at 20 MPa√m on heat N85426 (specimens CT189&90) when using active test management methods, it seems that usage of passively loaded specimens that cannot be load cycled to recover a stalled crack do not provide an adequate opportunity to effectively assess low K CISCC response. Thus, it could be expected that the apparent, and possibly incorrect, threshold stress intensity for crack growth might vary from study-to-study. This appears to be the case when reviewing the relevant literature. In boiling NaCl-saturated water, Speidel **[23]** observed a threshold K for CISCC growth of ~37 MPa√m for 304, ~20 MPa√m for 304L, and ~27 MPa√m for 316L. Shaikh, et al. **[24]** also conducted SCC tests as a function of K in boiling NaCl solutions on 304N and 316 using bolt loaded and constant load specimens. The threshold stress intensity for crack growth was 17 MPa√m for 304N, 11 MPa√m for sensitized 304N, 13 MPa√m for 316, and 10.5 MPa√m for sensitized 316, all of which are lower than what was reported by Speidel. Kosaki **[25]** conducted CGR versus K testing in deliquescent

humid air conditions using a 3-point bend method. CISCC growth was observed for K values as low as 1 MPa√m. Kosaki's results showing growth at stress intensities of 1 MPa√m is rather surprising, and since the method by which K was calculated was not mentioned in the paper, the accuracy of the K values is unknown. When these results are reviewed in aggregate, a wide range of threshold values are observed. This may simply be due to passive test management and the use of relatively low resolution methods for measuring crack length. One additional point to make in regard to threshold behavior is that Speidel and Shaikh obtained their data in boiling NaCl while Kosaki's data was obtained at temperatures as low 22°C. Thus, the current literature data does not indicate that the threshold stress intensity, if it exists, varies with temperature.

A plot of CISCCGR versus stress intensity at 40°C in NaCl for the PNNL tests to-date is provided in Figure 45. At this time, there is insufficient data to establish any particular trend with stress intensity, but until there are sufficient data, PNNL is taking the approach of assuming that there is no threshold stress intensity and that crack growth will occur as a function of stress intensity all the way down to very low K values. The current stress exponent is ~1.8, and extrapolation of the power law curve fit projects that the crack growth rate will drop to $1x10^{-9}$ mm/s (~30 µm/yr) at ~2 MPa√m. It is highly likely that this assessment will change substantially as more data are obtained at progressively lower stress intensities.

Another aspect of the early test results that is interesting to consider is the effect of sensitization on crack growth. In the work of Shaikh **[24]**, sensitized material was found to have a lower threshold stress intensity and higher crack growth rate than non-sensitized material. The sensitized 304 being tested by PNNL thus far has a slightly lower SCCGR than non-sensitized 304L. The lower SCCGR for sensitized material tested by PNNL doesn't necessarily conflict with the work of Shaikh, but rather it serves to show that the effect of sensitization on CISCC growth may be no stronger than heat-to-heat variability or the effect of the slight compositional difference between 304 and 304L.

Another comment is that that the relatively similar CISCCGRs between the 304L and the sensitized 304 suggest similar SCC cracking morphology, likely transgranular SCC.

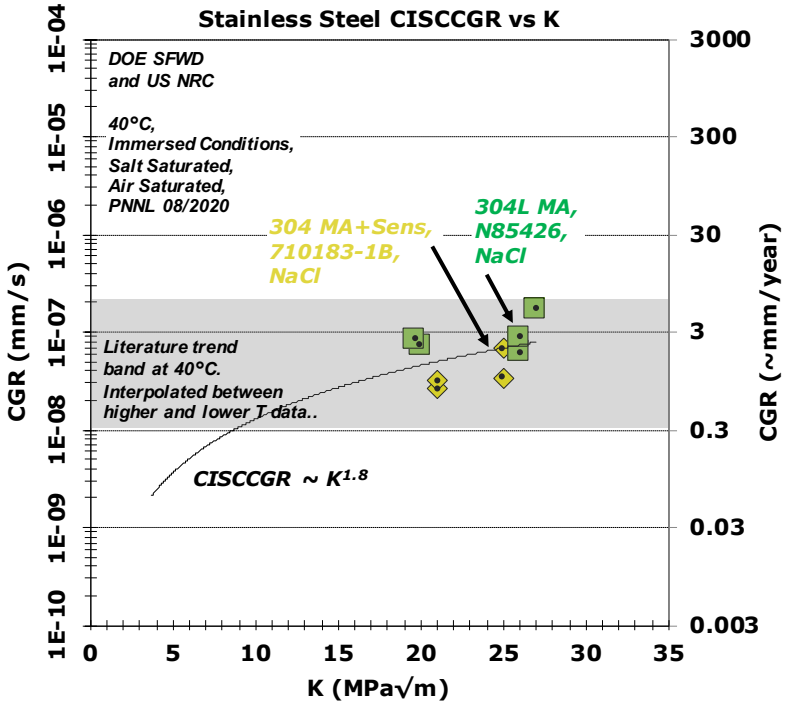

Figure 45. CISCCGR response versus K at 40°C in NaCl for two heats of stainless steel.

This page is intentionally left blank.

8. Summary

The majority of the research effort this fiscal year involved constructing the second two CISCC test systems and refining the ability of all four PNNL test systems to produce high quality data with well controlled water chemistry. All four test systems are now fully operational, and in late FY20, high volume CISCC growth rate testing in immersed conditions will begin in the CISCC3 and CISCC4 test systems on task materials while testing will continue in CISCC1 and CISCC2 on non-task specimens that were readily available before task materials had been selected.

Three task materials – two heats of 304L and one heat of 316L – were procured, characterized, and prepared for testing this year. One key factor in the material selection was obtaining materials with high strength in the as-produced condition because higher strength materials tend to exhibit higher SCC susceptibility. It is pertinent to focus on materials with high as-produced strength because container vendors are not required to select low strength materials, making it virtually assured that some of their stock is made from 304/316 stainless steel on the higher end of the strength spectrum. The other key factor in selection of the 304L was obtaining two heats of different composition while staying within the composition specification. For this aspect, the primary difference in composition between the two 304L heats is Molybdenum content. The ASTM standard for 304/304L composition does not specify a Mo content range, and typically low Mo content is used. One heat has a Mo content of 0.1 wt% while the other has a Mo content of 0.41 wt%. Mo is generally considered to improve corrosion resistance, but to obtain this benefit, additional austenite stabilizing elements must be added to the alloy to prevent a greater tendency for ferrite/martensite formation that is detrimental to corrosion resistance. This is the approach used to make 316/316L, but for 304/304L, no effort is made to adjust the content of austenite former elements when the Mo content is higher. This can lead to a material this is actually more susceptible to SCC.

CISCC growth rate tests on two specimens was completed and tests are underway on four more specimens. The aim of these initial tests has been to use these to evaluate and refine test systems capability while obtaining CISCC growth rate versus stress intensity data that is needed to effectively evaluate the potential CISCC cracking response of stainless steel containers that are in service. All cracks start at relatively low stress intensity, so there is substantial value in understanding the dependence of growth rate on stress intensity. The available literature indicates that stainless steels exhibit a threshold response above which growth is relatively independent of K and below which there is essentially no growth. However, the threshold values reported in the literature vary widely from as little as 1 MPa$\sqrt{m}$ that is easily attained for very shallow cracks to more than 30 MPa$\sqrt{m}$ that is only possible for relatively deep cracks. Thus, there is a need to independently evaluate the stress intensity dependence and threshold response. The ongoing testing is evaluating response at progressively lower K values, which indicates that relatively high CISCC growth rates in 304 and 304L can be attained down to at least 20 MPa$\sqrt{m}$. Testing will continue on these four specimens while at the same time, additional testing will start on the task materials initially focused on evaluating CISCCGR as a function of stress intensity for non-cold worked and 10% cold worked materials.

For FY21, high volume CISCC growth rate testing will be undertaken in all four PNNL CISCC test systems. The aim will be to run 6-specimen tests in each system where duplicate specimens of each of the three task materials will be used to evaluate different environmental conditions as described in the FY19 PNNL CISCC test plan document. As described in that document, CISCC growth rate as a function of stress intensity, temperature, salt composition, salt concentration will all be evaluated in immersed conditions were a stable crack tip environment is much more easily attained compared to deliquescent humid air conditions. These results will serve as a basis for understanding test data obtained in deliquescent humid air conditions that is planned in following years.

This page is intentionally left blank.

9. REFERENCES

1. S. M. Bruemmer and M. B. Toloczko, “Pacific Northwest National Laboratory Investigation of Stress Corrosion Cracking in Nickel-Base Alloys”, NUREG/CR-7103, Volume 1, Nuclear Regulatory Commission, Office of Nuclear Regulatory Research, May 2011.
2. M.B. Toloczko, M.J. Olszta, Z. Zhai, S.M. Bruemmer, “Stress Corrosion Crack Initiation Measurements of Alloy 600 in PWR Primary Water”, Proceedings of the 17th International Conference on Environmental Degradation of Materials in Nuclear Power Systems – Water Reactors, August 9-12, 2015.
3. M.B. Toloczko, “Materials Reliability Program: Stress Corrosion Crack (SCC) Initiation Testing of Ni-Base Alloys for PWR Applications – Part 1 (MRP-426)”, Electric Power Research Institute (EPRI), Document #3002010761, 2017.
4. M.B. Toloczko, J.E. Smart, J.E. Deibler, R.J. Seffens, R.A. Bouffioux, “Chloride-Induced Stress Corrosion Cracking Test System Construction and Test Plan”, Pacific Northwest National Laboratory, PNNL-29166, 2019.
5. Materials Reliability Program (MRP) Crack Growth Rates for Evaluating Primary Water Stress Corrosion Cracking (PWSCC) of Thick-Wall Alloy 600 Materials (MRP-55) Revision 1. EPRI, Palo Alto, CA: 1006695, 2002.
6. Materials Reliability Program: Crack Growth Rates for Evaluating Primary Water Stress Corrosion Cracking (PWSCC) of Alloy 82, 182, and 132 Welds (MRP-115). EPRI, Palo Alto, CA: 1006696, 2004.
7. Materials Reliability Program: Recommended Factors of Improvement for Evaluating Primary Water Stress Corrosion Cracking (PWSCC) Growth Rates of Thick-Wall Alloy 690 Materials and Alloy 52, 152, and Variants Welds (MRP-386), Electric Power Research Institute (EPRI), Document 3002010756, 2017.
8. K. Shirai, J. Tani, T. Saegusa, "Study on Interim Storage of Spent Nuclear Fuel by Concrete Cask for Practical Use -- Feasibility Study on Prevention of Chloride Induced Stress Corrosion Cracking for Type 304 Stainless Steel Canister” (English translation), CRIEPI N10035, 2011.
9. J. Tani, M. Mayuzumi, N. Hara, “Initiation and Propagation of Stress Corrosion Cracking of Stainless Steel Canister for Concrete Cask Storage of Spent Nuclear Fuel”, Corrosion, Vol. 65, No. 3, 2009, pp. 187-194.
10. M.B. Toloczko, N.R. Overman, M.J. Olszta, and S.M. Bruemmer, “Pacific Northwest National Laboratory Investigation of Stress Corrosion Cracking in Nickel-Base Alloys, Part 3”, NUREG/CR-7103, Volume 3, July 2016.
11. P. Pedeferri (Deceased), “Stress Corrosion Cracking and Corrosion-Fatigue”, In Corrosion Science and Engineering, Engineering Materials, Springer, 2018, https://doi.org/10.1007/978-3-319-97625-9_13
12. M.B. Toloczko, J.E. Deibler, J.E. Smart, R.A. Bouffioux, “PNNL 4-Point Bend SCC Test Method Development for the U.S. Nuclear Regulatory Commission”, PNNL-29710, 2020.
13. National Institute of Standards and Technology (NIST) Chemistry WebBook, SRD 69, https://doi.org/10.18434/T4D303.
14. P.J. Meadows, P.L. Andresen, M.B. Toloczko, W.-J. Kuang, S. Ritter, M. Bjurman, L. Zhang, M. Ernestova, A. Toivonen, F. Perosanz-Lopez, J.W. Stairmand, K.J. Mottershead, “International Round-Robin on Stress Corrosion Crack Initiation of Alloy 600 Material in Pressurized Water Reactor Primary Water”, CORROSION. 2020;76(8):719-733.

15. Z. Zhai, M.B. Toloczko, S.M. Bruemmer, “Microstructural Effects on SCC Initiation in PWR Primary Water for Cold-Worked Alloy 600”, *Proceedings of the 18th International Conference on Environmental Degradation of Materials in Nuclear Power Systems – Water Reactors*, The Minerals, Metals & Materials Series, 2017, https://doi.org/10.1007/978-3-319-67244-1_14
16. Standard Specification for Chromium and Chromium-Nickel Stainless Steel Plate, Sheet, and Strip for Pressure Vessels and for General Applications, ASTM Standard A240, ASTM International, 100 Barr Harbor Drive, PO Box C700, West Conshohocken, PA.
17. E. Jafari, “Corrosion Behaviors of Two Types of Commercial Stainless Steel after Plastic Deformation, J. Mater. Sci. Technol., 2010, 26(9), 833-838.
18. Alloy Digest Sourcebook: Stainless Steels, ASM International, 2000.
19. D. Raabe, “Microstructure and Crystallographic Texture of Strip-Cast and Hot-Rolled Austenitic Stainless Steel”, METALLURGICAL AND MATERIALS TRANSACTIONS A, VOLUME 26A, APRIL 1995, p. 991.
20. C.A. Bryan, D. Enos, “Summary of available data for estimating chloride-induced SCC crack growth rates for 304/316 stainless steel” Sandia National Laboratories, SAND2016-2992R, 2016.
21. M. Creager, P.C. Paris, “Elastic field equations for blunt cracks with reference to stress corrosion cracking”, International journal of fracture mechanics, 3(4), 1967, pp. 247-252.
22. I.M Austen, R. Brook, and J.M. West. "Effective stress intensities in stress corrosion cracking." International Journal of Fracture 12.2, 1976, pp. 253-263.
23. M. Speidel, “Stress Corrosion Cracking of Stainless Steels in NaCl Solutions”, Met Trans A, 12A, 1981, pp. 779-789.
24. H. Shaikh, H. Khatak, P. Rodriquez, “Stress Corrosion Crack Growth Behavior of Austenitic Stainless Steels in Hot Concentrated Chloride Solution”, proceedings of ICF10 Meeting, Honolulu, 2001.
25. A. Kosaki, “Evaluation Method of Corrosion Lifetime of Conventional Stainless Steel Canister Under Oceanic Air Environment”, Nuclear Engineering and Design, 238, 2008, pp. 1233-1240.